

1 **Scattering and absorption properties of near-surface aerosol over Gangetic-Himalayan**
2 **region: the role of boundary layer dynamics and long-range transport**

3 **U. C. Dumka^{1*}, D. G. Kaskaoutis², M. K. Srivastava³ and P. C. S. Devara⁴**

4 ¹Aryabhata Research Institute of Observational Sciences, Nainital, India

5 ²Department of Physics, School of Natural Sciences, Shiv Nadar University, Tehsil Dadri, India

6 ³Department of Geophysics, Banaras Hindu University, Varanasi, India

7 ⁴Amity Centre for Ocean-Atmospheric Science and Technology (ACOAST), Amity University
8 Haryana, Gurgaon (Manesar), India

9 *Correspondence to: U. C. Dumka (dumka@aries.res.in; ucdumka@gmail.com)

10 **Abstract**

11 Light scattering and absorption properties of atmospheric aerosols are of vital importance in
12 evaluating their types, sources and radiative forcing. This is of particular interest over the
13 Gangetic-Himalayan (GH) region due to uplift of aerosol from the plains to the Himalayan range
14 causing serious effects on atmospheric heating, glaciology and monsoon circulation. In this
15 respect, Ganges Valley Aerosol Experiment (GVAX) was initiated at Nainital during June 2011
16 to March 2012 aiming to examine the aerosol properties, source regions, uplift mechanisms and
17 aerosol-radiation-cloud interactions. The present study examines the temporal (diurnal, monthly,
18 seasonal) evolution of scattering (σ_{sp}) and absorption (σ_{ap}) coefficients, their wavelength
19 dependence, and the role of the Indo-Gangetic plains (IGP), boundary-layer dynamics (BLD) and
20 long-range transport (LRT) in aerosol evolution via the Atmospheric Radiation Measurement
21 Mobile Facility. The analysis is separated for particles $<10 \mu\text{m}$ and $<1 \mu\text{m}$ in diameter in order to
22 examine the influence of the particle size on optical properties. The σ_{sp} and σ_{ap} exhibit a
23 pronounced seasonal variation with monsoon low and post-monsoon (November) high, while the
24 scattering wavelength exponent exhibits higher values during monsoon, in contrast to the
25 absorption Ångström exponent which maximizes in December-March. The elevated-background
26 measuring site provides the advantage of examining the LRT of natural and anthropogenic
27 aerosols from the IGP and southwest Asia and the role of BLD in the aerosol lifting processes.
28 The results reveal higher aerosol concentrations during noontime along with increase in mixing
29 height suggesting influence from IGP. The locally-emitted aerosols present higher wavelength
30 dependence of the absorption during October to March period compared to the rather well-mixed
31 and aged transported aerosols. Monsoon rainfall and seasonally-changing air masses contribute
32 to the alteration of the extensive and intensive aerosol properties.

35 **1. Introduction**

36 Light scattering and absorption by atmospheric aerosol cause reduction in solar radiation
37 reaching the ground and deterioration of visibility and air quality, modifying the atmosphere's
38 radiative and energy budget (Antón et al., 2012). The backscattering ratio is a crucial variable for
39 quantifying the cooling effect of aerosols on climate. Although it is weakly dependent on aerosol
40 concentration, it provides useful information of the refractive index, angular dependence of
41 scattering, size and shape of aerosols (Gopal et al., 2014). Wide-spread aerosol pollution mostly
42 from anthropogenic sources is a common phenomenon over the south Asia, with serious effects
43 on atmospheric circulation, climate and human health (Lawrence and Lelieveld, 2010 and
44 references therein). This aerosol-pollution layer, especially over the Indo-Gangetic Plains (IGP),
45 is clearly observed by the satellite imagery as a thick haze layer (Atmospheric Brown Clouds,
46 ABC) over the region (Di Girolamo et al., 2004; Ramanathan et al., 2007), spreading also over
47 the Himalayas with significant light absorption due to large Black Carbon (BC) concentration
48 (Adhikary et al., 2007; Nakajima et al., 2007; Kopacz et al., 2010; Gautam et al., 2011).

49
50 During the last decades, the IGP has experienced increasing aerosol and pollutant emissions
51 mainly from anthropogenic sources, fossil-fuel and bio-fuel combustion and agricultural biomass
52 burning (Lu et al., 2011; Kaskaoutis et al., 2012), which along with the natural dust emissions
53 and long-range transport (LRT) have led to severe turbid atmospheres (Kaskaoutis et al., 2013).
54 As a consequence, aerosols can strongly modify the regional climate via radiative forcing
55 (Ramanathan et al., 2005; Lau et al., 2006; Gautam et al., 2010) and changes in cloud
56 microphysics, monsoon rainfall and dynamics (Randles and Ramaswamy, 2008, BOLLASINA and
57 NIGAM, 2009; Ganguly et al., 2012; Manoj et al., 2011; Dipu et al., 2013). Due to their
58 significant influence on regional weather, climate, monsoon circulation, glaciology and human
59 health, aerosols are systematically examined over Indian Himalayas, mostly focusing on
60 columnar properties and radiative forcing (Dumka et al., 2006, 2008; Hegde et al., 2007; Guleria
61 et al., 2011 and reference therein) and a few studies on aerosol chemistry (Ram et al., 2008,
62 2010; Hegde and Kawamura, 2012). In contrast, systematic analysis of near-surface aerosol
63 properties is sparse and mostly performed under an Indian-Finish research initiative (Hyvärinen
64 et al., 2009, 2011a, 2011b). Furthermore, Raatikainen et al. (2014) examined the influence of
65 boundary-layer dynamics (BLD) and the effect of changes in boundary-layer height (BLH) on
66 aerosol concentrations over the IGP and their transport up to the Himalayan foothills. Panwar et
67 al. (2013) analyzed the evolution of the PM and BC aerosol mass concentrations at Mukteshwar
68 with respect to seasonal variations of BLH, while Komppula et al. (2009) and Neitola et al.
69 (2011) focused on the aerosol size distribution and new particle formation at the same site. These

70 studies corroborate larger aerosol concentrations and new particle formation during the spring
71 period associated with higher BLH and increased influence of transported aerosols.

72
73 To improve the knowledge of radiative properties of atmospheric aerosols, their origin and
74 spatio-temporal distribution over the Gangetic-Himalayan (GH) region, the Ganges Valley
75 Aerosol Experiment (GVAX) was initiated during June 2011 to March 2012 (Kotamarthi and
76 Satheesh, 2011). The GVAX project was a joint research campaign between US Department of
77 Energy (DoE) Atmospheric Radiation Measurement (ARM) Program and Indian Institute of
78 Science, Bangalore conducted at Manora Peak, Nainital, in the central part of Indian Himalayas
79 (29.21° N, 79.27° E, 1958 m a.m.s.l). Based on GVAX measurements, Manoharan et al. (2014)
80 analyzed the aerosol properties, mostly emphasizing on the higher absorption of the super-
81 micron (1-10 μm) particles during October-November accounting for 44% of the total aerosol
82 radiative forcing. Dumka and Kaskaoutis (2014) examined the variation of the single scattering
83 albedo (SSA) during GVAX and its contribution to the aerosol radiative forcing efficiency
84 depending on particle size, also discussing some preliminary results of the monthly variation of
85 scattering and absorption coefficients. More recently, Dumka et al. (2015) analyzed the cloud
86 condensation nuclei (CCN) variations and examined the activation of aerosol particles to CCN as
87 a function of season, LRT and BLD.

88
89 The present work aims to a comprehensive investigation of the intensive and extensive aerosol
90 properties (scattering, backscattering and absorption coefficients, their wavelength dependence
91 and relationships between them) as a function of particle size ($D_{10\mu\text{m}}$ and $D_{1\mu\text{m}}$) over the GH
92 region during the GVAX campaign. The main objective is to shed light in the temporal (diurnal,
93 monthly, seasonal) evolution of the near-surface aerosol properties and the specific role of the
94 BLD, uplift of aerosols, LRT and rainy washout. The nearly background measuring site
95 (Nainital), gives us the possibility of exploring the specific role of aerosol-pollution uplift from
96 the IGP to the Himalayan foothills and the seasonal influence of LRT on aerosol optical
97 properties.

98
99 **2. Measurements and data analysis**

100 **2.1. Observational site**
101 The aerosol measurements were conducted by DoE/ARM Mobile Facility (AMF) deployed at the
102 mountain-top (1958 m amsl) Manora Peak, Nainital, in the GH region (Dumka and Kaskaoutis,
103 2014). The observational site is far from any major pollution sources, such as industrialized areas
104 and metropolitan cities, with a total population of ~0.5 million and density of ~50 people per km^2

105 (census 2011). The site is bounded by high-altitude mountain peaks in the north and east
106 directions and opens to the IGP region (densely populated, high polluted and aerosol laden) in
107 the south and west. By considering the elevated nature of the site, the growth of planetary
108 boundary layer (PBL) in the early afternoon hours (usually up to 3-3.5 km amsl) plays a major
109 role in bringing-up aerosols from the IGP, causing significant perturbations in atmospheric
110 physics and chemistry (Dumka et al., 2010; Prabha et al., 2012). The major aerosol sources at
111 Nainital during winter are local/regional biomass-burning emissions (domestic use and heating
112 purposes) and transport of pollutants from the IGP (Dumka et al., 2008). During pre-monsoon
113 (March–May), the site is influenced by transported dust plumes from Thar desert and southwest
114 Asia (Hegde et al., 2007; Kumar et al., 2014) with a relative decrease in carbonaceous aerosols
115 (Ram et al., 2008), while in post-monsoon, smoke-laden air masses from agricultural crop-
116 residue burning in Punjab affect the site. Rain-washout process during the monsoon period
117 decreases the aerosol concentration.

118

119 **2.2. Measurements and techniques**

120 In-situ measurements of near-surface aerosol absorption (σ_{ap}) and scattering (σ_{sp}) coefficients
121 were carried out using the aerosol observing system (AOS) (Sheridan et al., 2001; Jefferson,
122 2011, and references therein). The AOS was housed in an air conditioned trailer and aerosol
123 samples were obtained from the top of a stainless steel intake stack (20.3 cm inner diameter),
124 protected with a rain cap. The aerosols were passed from the stack through a manifold and into
125 several sampling lines that deliver the sample air to the various instruments. Each aerosol sample
126 passes through switched impactors that toggle the aerosol size cut between 1.0 μm ($D_{1\mu\text{m}}$) and 10
127 μm ($D_{10\mu\text{m}}$) aerodynamic particle diameters every 30 minutes, thus allowing the examination of
128 both fine and coarse particles (Jefferson, 2011). The AOS instrumentation that is used in the
129 current work consists of Nephelometer and Particle Soot Absorption Photometer (PSAP) from
130 which several extensive and intensive aerosol properties have been analyzed (see Table 1).

131

132 The σ_{ap} was measured via the three wavelengths (0.47, 0.53 and 0.66 μm) PSAP. The PSAP uses
133 a filter-based technique in which aerosols are continuously deposited onto a glass fibre filter and
134 the change in the transmitted light is related to the σ_{ap} of the deposited particles using the
135 Lambert Beer's law (Bond et al., 1999). Absorption data with filter transmissions below 0.7 were
136 rejected in this study, while the data averaging time was 1 minute. The response of PSAP
137 depends on aerosol loading on the filter, amount of light scattered by particles, flow rate (~0.8
138 lpm) and spot size (Virkkula et al., 2011). Following the methodology from previous works
139 (Bond et al., 1999; Ogren, 2010), the raw PSAP data were processed to estimate the σ_{ap} by

140 incorporating the sample area, flow rate and spot size calibrations. Other biases are due to the
141 scattering and multi-sample loading on the filter, instrument noise (~6% of total absorption,
142 [Bond et al., 2001](#)) and uncertainty in the PSAP measurements (1 to 4 Mm^{-1} for the 1-min
143 averaged data samples, [Manoharan et al., 2014](#)). The total uncertainty of the PSAP
144 measurements after the transmission and scattering correction is ~20-30% ([Bond et al., 1999](#)).

145

146 The total scattering (σ_{sp} ; between 7° and 170°) and hemispheric backscattering (σ_{bsp} ; between 90°
147 and 170°) coefficients at three wavelengths (0.45, 0.55 and 0.70 μm) were measured with an
148 integrating Nephelometer (Model 3563, TSI). The Nephelometer operated at a relative humidity
149 (RH) below 40% to minimize the effects of changing RH on measurements, while a second
150 Nephelometer was also connected to a humidity scanning system to provide measurements of σ_{sp}
151 and σ_{bsp} as a function of RH for studying the light scattering enhancement factor (work under
152 preparation). The angular non-idealities (i.e. truncation error) and non-Lambertian light source
153 were corrected following the methodology described by [Anderson and Ogren \(1998\)](#) and details
154 are given in [Dumka and Kaskaoutis \(2014, and references therein\)](#). The averaging time was set to
155 1 min, and the Nephelometer was calibrated using CO_2 as high span gas and air as low span gas.
156 On an average, the calibration constant is within $\pm 2\%$ and the overall uncertainty in the σ_{sp} is
157 ~7% ([Heintzenberg et al., 2006](#)). However, as noticed at the end of the campaign, the CO_2 was of
158 low quality to produce an accurate calibration, thus increasing the uncertainty of the
159 Nephelometer measurements to 10-15%.

160

161 The aerosol coefficients σ_{sp} , σ_{bsp} and σ_{ap} measured directly by the AOS are referred as “extensive
162 properties”, because they are mainly pertain to the amount of aerosols in the atmosphere. These
163 measurements were used to determine several other aerosol variables (known as “intensive
164 properties”), such as scattering Ångström exponent (SAE), back-scattering Ångström exponent
165 (BAE), absorption Ångström exponent (AAE), hemispheric backscatter fraction (b), sub-micron
166 scattering (R_{sp}) and absorption (R_{ap}) fractions, which are involved in the radiative forcing
167 estimations, rather than being related directly to the aerosol loading ([Table 1](#)). Therefore, the
168 intensive properties relate more to the character of aerosols, such as albedo, particle size and
169 hygroscopic behavior.

170

171 **3. Results and discussion**

172 **3.1. Variations in meteorological variables**

173 In terms of weather conditions and climatology, the observational site is characterized by four
174 different seasons: winter (December-January-February; DJF), spring/pre-monsoon (March-April-

175 May; MAM), summer/monsoon (June-July-August-September; JJAS) and autumn/post-monsoon
176 (October-November; ON). The ambient pressure, temperature (Temp), relative humidity (RH),
177 wind speed (WS) and wind direction (WD) were continuously monitored during the study period
178 (June 2011 to March 2012) using the surface meteorological instrumentation (MET) data from
179 the ARM AMF facility.

180

181 The ambient atmospheric pressure varies between 79 and 81 Kpa, gradually increasing from
182 monsoon to winter and then, slightly decreasing towards spring (Fig. 1a). The monthly-mean
183 temperature remains nearly steady (~ 20 °C) between June and September, with a gradual
184 decrease thereafter to a minimum value of ~ 7 °C in January (Fig. 1b). The RH is greater than
185 90% during summer monsoon and decreases to about 60% to 40% during the rest of the period,
186 also exhibiting larger fluctuation due to changing weather conditions involving arrival of humid
187 or dry air masses (Fig. 1c). In general, the wind speed (Fig. 1d) varies between 2 and 6 m s⁻¹ with
188 an average of ~ 2 m s⁻¹ for most of the time. Westerly-to-northwesterly winds (Fig. 1e) dominate
189 during October-March period, carrying aerosols and pollutants from western IGP and southwest
190 Asia. June is mostly considered as a transition month with changing wind from westerly to
191 easterly, while the mean wind direction from July to September is easterly to south-easterly
192 associated with increased monsoon rainfall.

193

194 **3.2. Temporal evolution of near-surface aerosol properties**

195 This section analyzes the temporal evolution of near-surface aerosol properties at Nainital and
196 discusses them as a function of wavelength, particle size and prevailing atmospheric and
197 meteorological conditions.

198

199 **3.2.1. Extensive properties**

200 The mean values (averaged on seasonal basis and during the entire study period) of σ_{sp} , σ_{bsp} and
201 σ_{ap} along with their wavelength dependencies are summarized in Table 2 for both $D_{1\mu m}$ and $D_{10\mu m}$
202 particles in order to reveal the influence of particle size on aerosol extensive and intensive
203 properties.

204

205 The average σ_{sp} and σ_{ap} during the whole study period were found to be 177.2 Mm⁻¹ and 13.5
206 Mm⁻¹, respectively, for the $D_{10\mu m}$ and 104.4 Mm⁻¹ and 8.9 Mm⁻¹ for the $D_{1\mu m}$ (Table 2), with
207 significant seasonal variation (post-monsoon high and monsoon low). The mean value of σ_{sp} is
208 similar to earlier observations over the site (Pant et al., 2006; Beegum et al., 2009). The σ_{sp}
209 values over central Indian Himalayas (present study and Hyvärinen et al. 2009) are comparable

210 to those found over central India during February 2004 (Jayaraman et al., 2006), but much lower
211 than those ($250 - 2000 \text{ Mm}^{-1}$) reported at polluted Indian megacities, like Delhi (Ganguly et al.,
212 2006). The scattering is $\sim 40\%$ larger for the $D_{10\mu\text{m}}$, especially at longer wavelengths, while the
213 σ_{bsp} varies from ~ 5 to 23 Mm^{-1} (~ 3 to 14 Mm^{-1}) for $D_{10\mu\text{m}}$ ($D_{1\mu\text{m}}$), respectively on monthly basis.
214 The σ_{bsp} follows the seasonal variation of σ_{sp} with larger values in November (~ 0.23 and ~ 0.13
215 for $D_{10\mu\text{m}}$ and $D_{1\mu\text{m}}$, respectively) and lowest in monsoon. The monthly variations of the spectral
216 σ_{sp} and σ_{ap} were documented in Dumka and Kaskaoutis (2014). Manoharan et al. (2014) reported
217 a 30% greater absorption for $D_{10\mu\text{m}}$ compared to $D_{1\mu\text{m}}$ during October–November 2011, in
218 contrast to the similar values (7.63 ± 5.32 and 6.38 ± 3.91 for $D_{10\mu\text{m}}$ and $D_{1\mu\text{m}}$, respectively)
219 found during monsoon. The post-monsoon season coincides with the post-harvest agricultural
220 biomass burning period in Punjab, northwestern India (Kaskaoutis et al., 2014), implying that the
221 absorbing aerosols can be also of larger size due to atmospheric mixing and ageing processes
222 (gas-to-particle conversion, coagulation, condensation) during their transportation up to Nainital.
223 These aerosols are mostly emitted over IGP, whereas the local freshly-emitted aerosols at
224 Nainital (mostly in the $D_{1\mu\text{m}}$ size) seem not to affect so much the light absorption due to their
225 significantly lower abundance (Hyvärinen et al., 2009; Ram et al., 2010). It should be noted that
226 the difference in absorption coefficient between $D_{10\mu\text{m}}$ and $D_{1\mu\text{m}}$ is larger for higher aerosol
227 loading during post-monsoon and March.

228
229 Higher values of σ_{bsp} ($14 \pm 1 \text{ Mm}^{-1}$) and b (~ 0.13) at 550 nm compared to Nainital were found in
230 Anantapur, south India during January – December 2011 (Gopal et al., 2014), suggesting
231 dominance of different aerosol types associated with lower aerosol loading (mean σ_{sp} of 97 ± 9
232 Mm^{-1}). σ_{sp} value of $75 \pm 42 \text{ Mm}^{-1}$ at 550 nm was reported by Andreae et al. (2002) at Sde Boker,
233 Israel, which was typical of moderate-polluted continental air masses, while values of 26 Mm^{-1}
234 and 410 Mm^{-1} were found for clean and heavy-smog days, respectively, in Los Angeles (Seinfeld
235 and Pandis, 1998). Table 3 summarizes the extensive and intensive aerosol properties over
236 Nainital during the GVAX campaign along with those measured over mountainous and remote
237 sites over the globe. The comparison shows that Nainital, although its elevated terrain and
238 remoteness from urban and industrialized regions, usually receives substantial amounts of
239 anthropogenic aerosols, in addition to mineral dust and biomass burning, rendering the site as
240 moderately polluted.

241

242 3.2.2. Intensive properties

243 The monthly values of SAE determined at three spectral bands are shown in Fig. 2 exhibiting a
244 similar temporal variation for both $D_{1\mu\text{m}}$ and $D_{10\mu\text{m}}$ size groups, but with much larger values for

245 the $D_{1\mu\text{m}}$ (mean of 1.21 ± 0.35 at $0.45\text{-}0.70 \mu\text{m}$) compared to $D_{10\mu\text{m}}$ (mean of 0.72 ± 0.42 at 0.45-
246 $0.70 \mu\text{m}$) (Table 2). The wide range (~ 0.1 to 2.4) of SAE values for both particle groups suggests
247 large variability in sources, seasonality and mixing processes at the measuring site. The average
248 value of SAE at $0.45\text{-}0.70 \mu\text{m}$ was found to be 1.02 ± 0.30 at Anantapur (Gopal et al., 2014),
249 which is well within the average values of $D_{1\mu\text{m}}$ and $D_{10\mu\text{m}}$ at Nainital. Furthermore, the SAE
250 values are higher at the shorter wavelength bands, suggesting higher decreasing rate of the
251 scattering process at shorter wavelengths, as expected from the Mie theory. Previous work
252 (Dumka and Kaskaoutis 2014) showed a similar annual pattern of σ_{sp} and σ_{ap} for both $D_{1\mu\text{m}}$ and
253 $D_{10\mu\text{m}}$ particles. The present analysis revealed different values and wavelength dependence,
254 indicating that the particle size plays a prominent role in altering the aerosol optical properties.

255
256 The monthly variability depends on the dominant aerosol type, the contribution of local and
257 transported aerosols, the prevailing meteorological conditions and the mixing processes in the
258 atmosphere. The maximum monthly-mean SAE is observed in August (1.11 ± 0.31 and $1.53 \pm$
259 0.26 for $D_{10\mu\text{m}}$ and $D_{1\mu\text{m}}$, respectively) and, in general, the wavelength dependence of scattering
260 seems to be higher during monsoon (Table 2). The minimum values are shown in October and
261 November, when the site is under significant influence of the smoke-laden air masses from
262 northwestern India, and both scattering and absorption are at their highest levels (Manoharan et
263 al., 2014; Dumka and Kaskaoutis, 2014). Hyvärinen et al. (2009) found lowest values of Aitken-
264 to-Accumulation mode ratio during the pre- and post-monsoon seasons over central Indian
265 Himalayas indicating largest influence of LRT, which was also justified by the highest particle
266 number concentrations (Dumka et al., 2015). In contrast, during the monsoon season, the Aitken-
267 to-Accumulation mode ratio was higher due to more efficient removal of accumulation mode by
268 the rain-washout process, implying that the aerosols are of smaller size, less aged and mostly
269 freshly emitted, thus explaining the highest SAE values during July-September. The lowest SAE
270 in November is an indicator of the abundance of aged coarse aerosols, whereas the local primary
271 emissions are mostly at the Aitken size, thus contributing to the much larger SAE for the $D_{1\mu\text{m}}$
272 particles and to the general increase in SAE during winter due to the influence of bio-fuel
273 burning. Similar values of SAE, but with different annual pattern (maximum of 1.5 ± 0.1 in
274 January and minimum of 0.7 ± 0.1 in September), were found in Anantapur (Gopal et al., 2014)
275 indicating significant difference in source apportionment, influence of local emissions and
276 seasonal meteorological conditions between the GH region and the southern Indian peninsula.

277
278 The monthly variation of BAE is shown in Fig. 3, revealing a general agreement with SAE (Fig.
279 2) due to the reasons mentioned above. BAE exhibits significant spectral dependence with larger

280 values at shorter wavelengths (0.45-0.55 μm) and near zero to even negative values at 0.55-0.7
281 μm due to larger backscatter coefficient values at 0.7 μm in some months. Note also that the
282 negative $\text{BAE}_{0.55/0.7}$ values are more prominent for $\text{D}_{10\mu\text{m}}$ particles indicating the influence of the
283 particle size in the spectral backscatter coefficient. In contrast, for $\text{D}_{1\mu\text{m}}$ particles negative
284 monthly-mean $\text{BAE}_{0.55/0.7}$ values are shown only in October-November and March, i.e., the
285 months with the lowest SAE values (Fig. 2). $\text{BAE}_{0.45/0.7}$ is almost double for the $\text{D}_{1\mu\text{m}}$ particles
286 (Table 2) and, especially on seasons with dominance of coarse aged aerosols (pre-monsoon and
287 post-monsoon), the difference between $\text{D}_{1\mu\text{m}}$ and $\text{D}_{10\mu\text{m}}$ BAE values is even larger. This suggests
288 that BAE is more sensitive on particle size than SAE and can be used as an additional tool for
289 aerosol type discrimination. It was found (not presented) that BAE and SAE are highly linear
290 correlated to each other with R^2 of 0.8 (0.6) for $\text{D}_{10\mu\text{m}}$ ($\text{D}_{1\mu\text{m}}$) at 0.45-0.7 μm band, implying co-
291 variance in the wavelength dependence of scattering and backscattering.

292
293 The monthly variation of the spectral AAE exhibits similar pattern for both size groups with
294 larger values at shorter wavelengths (Fig. 4). However, the wavelength dependence of the AAE
295 strongly differentiates as a function of season and particle size. It is higher for $\text{D}_{10\mu\text{m}}$ particles
296 and increases from monsoon to winter and pre-monsoon (for both particle groups), suggesting
297 differences in the source regions and dominant aerosol type. The larger values and wavelength
298 dependence of AAE correspond to enhanced contribution of dust and carbonaceous aerosols
299 from biofuel burning, while values of AAE around 1 are characteristic of dominance of fossil-
300 fuel combustion (Kirchstetter et al., 2004). The highest wavelength dependence of AAE in
301 March is a fingerprint of the larger dust contribution either locally emitted or long-range
302 transported. The AAE for the $\text{D}_{1\mu\text{m}}$ is found to be slightly larger (mean of 1.14 ± 0.18 at 0.47-
303 0.60 μm) than that of $\text{D}_{10\mu\text{m}}$ (mean of 1.07 ± 0.20 at 0.47-0.60 μm), with a maximum during
304 December-March (~ 1.3) and minimum during monsoon (~ 1.0). Monthly-mean AAE values in
305 the range of 1.0 to 1.6 are reported at Mukteshwar, close to Nainital (Hyvärinen et al. 2009),
306 which are larger during winter, similarly to our results (Fig. 4). A wide range (from 0.16 to 2.16,
307 mean of 1.43 ± 0.41) in AAE values was also found by Andreae et al. (2002) indicative of very
308 contrasting air masses and aerosol absorption efficiencies in arid Israel. The AAEs for $\text{D}_{1\mu\text{m}}$ and
309 $\text{D}_{10\mu\text{m}}$ have shown a correlation coefficient of ~ 0.9 and most of the data points lie close to the 1-1
310 line (Manoharan et al., 2014), suggesting rather consistency in the aerosol source regions, and
311 negligible effect of the particle size. In synopsis, the increase in both absorption and scattering
312 coefficients during the last week of October and November due to enhanced biomass-burning
313 activity over northwestern India is generally associated with a weaker wavelength dependence of

314 both scattering (Fig. 3) and absorption (Fig. 4), suggesting an abundance of super-micron
315 aerosols that absorb in the whole spectrum (Manoharan et al., 2014).

316
317 The monthly evolution of the spectral backscatter fraction (b) is shown in Fig. 5 for both particle
318 sizes. The results show that the b is strongly wavelength dependent, with larger values at longer
319 wavelengths (opposite to that found for σ_{sp} and σ_{ap} , SAE and AAE). The larger SAE that was
320 found in monsoon (Fig. 2) indicates particles of smaller size, which are associated with more
321 isotropic scattering and usually higher b values, while forward scattering and smaller b values
322 are indicative of larger particles (Mie Theory). However, the results exhibit smaller b in
323 monsoon (Table 2), while from post-monsoon to March the b slightly increases (except of small
324 decreases in November and January). The highest b values are observed in March suggesting
325 more irregular type of scattering and favoring of backscatter, which is characteristic of the dust
326 particles (Liu et al., 2008). Lack of covariance between SAE and b is indicative of a bimodal size
327 distribution, which seems to be the usual scenario in our case. The b is larger at longer
328 wavelengths, especially for the $D_{1\mu m}$ particles, since the backscatter wavelength dependence is
329 lower than that of total scattering and, therefore, the backscatter-to-total scattering ratio (b) is
330 more enhanced at longer wavelengths. Slight higher b values are found for the sub-micron
331 particles over Nainital at 0.45 and 0.55 μm (Table 2), which become significantly higher at 0.7
332 μm compared to those of $D_{10\mu m}$ (Fig. 5). This is because the coarse particles favor the forward
333 scattering (i.e. larger asymmetry factor and smaller b) than the smaller particles. The b at 0.55
334 μm lies in the range 0.034-0.089 (0.027-0.100) with higher values in March 0.080 ± 0.005 (0.092
335 ± 0.006) and lower in August 0.054 ± 0.010 (0.058 ± 0.012) for $D_{10\mu m}$ ($D_{1\mu m}$). On average, the b
336 values at 0.55 μm were found to be 0.067 ± 0.009 for $D_{10\mu m}$ and 0.073 ± 0.012 for $D_{1\mu m}$, which
337 are much lower than those (0.13 ± 0.09) reported at Anantapur (Gopal et al., 2014), suggesting
338 presence of more aged aerosols and of larger size over Nainital. Backscatter ratio value of 0.13
339 was reported at the Negev desert, Israel under continental pollution conditions (Formenti et al.,
340 2001; Andreae et al., 2002), while similar values (0.14 ± 0.02) were found for polluted air
341 masses in the northwestern and eastern United States (Anderson et al., 1999; Sheridan and
342 Ogren, 1999). Previous studies (Carrico et al., 2003; Doherty et al., 2005) have shown that the b
343 values are higher for dust and biomass-burning aerosols, while they may be also sensitive to
344 composition (organic content and particle size distribution) of aerosol (Twardowski et al., 2001;
345 Boss et al., 2004).

346
347 Figure 6 shows the temporal evolution of the σ_{sp} and σ_{ap} for the sub-micron ($D_{1\mu m}$) particles as
348 fraction of the respective efficiencies of $D_{10\mu m}$ (i.e. $D_{1\mu m}/D_{10\mu m}$). The decreasing trend with the

349 wavelength for the sub-micron scattering fraction implies more wavelength sensitivity compared
350 to $D_{10\mu\text{m}}$, whereas it becomes rather neutral for the absorption, suggesting that the spectral
351 absorption is similar for both $D_{1\mu\text{m}}$ and $D_{10\mu\text{m}}$. The sub-micron absorption fraction is higher than
352 that of scattering suggesting that the SSA would be lower for $D_{1\mu\text{m}}$, as justified (SSA for $D_{1\mu\text{m}} =$
353 0.91 , SSA for $D_{10\mu\text{m}} = 0.93$) in a previous study (Dumka and Kaskaoutis, 2014).

354
355 Both absorption and scattering sub-micron fractions exhibit a similar pattern with higher values
356 during July-August, which are decreasing in the post-monsoon, increase again in December-
357 January and decrease in March. The larger SAE in monsoon (Fig. 2) implies abundance of fine
358 aerosols (large Aitken-to-Accumulation ratio, Hyvärinen et al., 2009) leading to enhanced sub-
359 micron scattering. The concurrent high values of sub-micron absorption fraction in July-August
360 suggest that either $D_{1\mu\text{m}}$ particles are more absorbing than the rest of the year or $D_{10\mu\text{m}}$ would be
361 less absorbing in monsoon. Sub-micron scattering and absorption are sensitive to the local
362 anthropogenic emissions (at the Aitken size) during the monsoon and winter months, thus
363 exhibiting higher fractions compared to the rest of the period. Except of the particle size and
364 shape that mostly define the scattering processes, the aerosol chemical composition plays a vital
365 role in the absorption efficiency. The carbonaceous aerosols were found to contribute about 25%
366 of the total aerosol mass in Nainital (Ram et al., 2010), while the WSOC/OC (water soluble
367 organic carbon/organic carbon) ratio (0.55 ± 0.15) was found to be larger than that over the IGP
368 locations, suggesting enhanced contribution from secondary organic aerosols (mostly in the
369 Aitken size). Concerning the coarse-mode particles, except of the LRT dust from the arid and
370 semi-arid regions in southwestern Asia (see Fig. 9), dust particles may originate from local wind-
371 blown dust, dust re-suspension due to road traffic or dust due to farming activities over the GH
372 region (Raatikainen et al., 2014).

373 374 **3.3. Diurnal cycle of aerosol properties**

375 The monthly-mean diurnal evolutions of σ_{sp} , σ_{ap} , SAE and AAE are shown in Fig. 7 (a-d),
376 respectively, for both $D_{1\mu\text{m}}$ and $D_{10\mu\text{m}}$. The σ_{sp} and σ_{ap} exhibit similar diurnal and seasonal
377 patterns, with post-monsoon to winter (and March) highs and monsoon lows. Both maxima are
378 observed in November due to significant influence of transported smoke from agricultural
379 burning (Dumka and Kaskaoutis, 2014), while a slight decrease is observed in January. Similar
380 annual variation of both σ_{sp} and σ_{ap} was reported at Mukteshwar (Hyvärinen et al. 2009). The
381 slight lower December-January values were attributed to the confinement of the IGP polluted
382 boundary layer below the site's altitude. Furthermore, synoptic-scale transport and changing air-
383 mass origin affect the aerosol loading over the Himalayan sites (Xu et al., 2014; Bucci et al.,

384 2014). The annual variation of the σ_{ap} seems to follow that of the BC mass fraction, which was
385 found to be ~1% during monsoon and 7.6% during winter (Ram et al., 2010), associated with
386 variation in σ_{ap} (at 0.678 μm) from 0.9 to 33.9 Mm^{-1} . However, no significant difference in σ_{ap}
387 and σ_{sp} was found between weekdays and weekends in contrast to Anantapur, where a 7.8%
388 reduction in σ_{sp} was reported in weekends (Gopal et al., 2014). The factor that seems to
389 contribute to the increase in σ_{sp} and σ_{ap} during noon to afternoon hours, is the slope up-stream of
390 the polluted air masses coming from the IGP after deepening ($> 2.5\text{-}3$ km) of the PBL over the
391 Ganges valley. Local-scale daily wind patterns, like valley wind cells, may also influence the
392 diurnal patterns of spectral σ_{sp} and σ_{ap} ; upslope winds are expected to increase the aerosol
393 loading over the site, while downslope winds result in atmospheric cleansing. Afternoon-to-
394 evening peaks in σ_{sp} and σ_{ap} were also reported at Mukteshwar during the post-monsoon and
395 winter seasons, which were vanished during monsoon (Hyvärinen et al. 2009).

396
397 The seasonal pattern of SAE reveals larger values during monsoon, which can be explained by
398 the rain washout of the coarser aerosols, and a secondary increase during December-January
399 mostly associated with local emissions from biofuel combustion (morning and evening maxima).
400 The diurnal variation observed in December-January is smoothed during the rest of the year for
401 both particle sizes. In contrast to SAE, the diurnal pattern of AAE exhibits significant variability
402 during October – March, indicating dominance of different aerosol types and mixing processes.
403 Higher AAE values ($>1.3\text{-}1.4$) are observed during night-to-early morning hours in the winter
404 season, while during noontime the AAE goes down to 1-1.2. Peaks in AAE during the morning
405 and evening hours were also found over Mukteshwar (Hyvärinen et al. 2009) suggesting
406 influence of local biomass burning, i.e. burning of leaves and wood for heating, which did not
407 contribute to the diurnal patterns of σ_{sp} and σ_{ap} (Fig. 7a, b), as they are mostly affected by the
408 LRT from IGP. The diurnal pattern of AAE reveals the dominance of different aerosol sources
409 and combustion processes, i.e. local emissions from biofuel burning in the early morning and
410 evening hours (high values of AAE) and transport of mostly aged aerosols from fossil-fuel
411 combustion in IGP during noon to early afternoon (low values of AAE) (Bergstrom et al., 2007).
412 In contrast, any diurnal pattern flattens out during monsoon, when the low AAE values (below 1)
413 are associated with lowest σ_{ap} .

414
415 Raatikainen et al. (2014) noted that during winter the air masses up to Himalayan sites travel at
416 higher altitudes than the maximum BLH (~1-1.5 km) over the IGP, thus not being able to carry
417 significant amount of aerosol and pollutants. Such pollution transportation is very much favored
418 during pre-monsoon when the BLH is at its maximum ($>3\text{-}3.5$ km) and the dilution of aerosols in

419 the vertical favors their uplift to Himalayan foothills. Therefore, the role of the IGP to the aerosol
420 concentrations over the Himalayas is strongly related to BLH and dynamics. [Figure 8](#)
421 summarizes the seasonal-mean diurnal variations of σ_{sp} , σ_{ap} , SAE and AAE for $D_{10\mu m}$ along with
422 that of BLH. The latter was obtained from HYSPLIT model in hourly basis using the Turbulent
423 Kinetic Energy (TKE) profile method ([Draxler et al., 2012](#)), supposing that the BLH is assigned
424 to the height at which TKE either decreases by a factor of two or to a value less than 0.21
425 (m^2/s^2). The BLH exhibits a pronounced diurnal variation in all seasons, especially in pre-
426 monsoon (March), when it can reach up to 2.7 km at early-afternoon hours. During nighttime and
427 early morning, the BLH is only few meters thus trapping aerosols and pollutants near the ground.

428
429 The diurnal variation of the σ_{sp} and σ_{ap} exhibits systematic increase during noon-to-early
430 afternoon hours, coinciding well with the maximum BLH. In contrast, numerous papers
431 ([Ganguly et al., 2006](#); [Beegum et al., 2009](#); [Srivastava et al., 2012](#); [Dumka et al., 2013](#); [Pathak et](#)
432 [al., 2013](#); [Gopal et al., 2014](#), and many references therein) have shown increased pollutant
433 (mostly emphasizing to BC) concentrations over Indian cities during early morning and evening
434 hours due to lower BLH and trapping of pollutants near the ground and lower concentrations
435 during noontime (maximum BLH) due to enhanced convection and dilution of pollutants. These
436 diurnal patterns correspond mostly to urban environments and enhanced local emissions. The
437 contrasting diurnal variation of σ_{sp} and σ_{ap} at Nainital suggests dominance of long-range
438 transported aerosols from the Ganges Basin and west Asia, since the uplift is favored by the
439 deeper mixing layer during noontime. Note also a small time lag between maximum in BLH and
440 aerosol scattering/absorption that exists 1-2 hours later. In contrast, the diurnal variation is nearly
441 vanished during monsoon due to rainy washout, which seems to smooth the effect of the LRT
442 and constitutes the most effective scavenging factor that controls the aerosol loading and
443 evolution. [Prabha et al. \(2012\)](#) revealed the removal of pollution from the IGP to higher
444 atmospheric levels in association with dynamically forced updrafts. Their results showed that the
445 valley pollution could be uplifted to heights above the haze layer, favored by the buoyancy
446 generated due to thermal heating of the surface during noon-to-early afternoon hours. [Similar](#)
447 [diurnal patterns of BC and aerosol concentrations were found over other Himalayan sites, like](#)
448 [Nepal Climate Observatory - Pyramid \(NCO-P\), Nepal, and Darjeeling, eastern Indian](#)
449 [Himalayas \(Marinori et al., 2010; Sarkar et al., 2014\).](#) In contrast, the diurnal patterns of SAE
450 and AAE do not exhibit significant variations in all seasons, although the slight higher values
451 observed during early morning suggesting local influence of fine freshly-emitted aerosols.

452

453 **3.4. The role of wind and LRT in aerosol properties**

454 The diurnal and seasonal evolution of the aerosol properties over Nainital is a function of the
455 emission sources, meteorological conditions (rainfall, wind pattern), BLD and LRT. In this
456 respect, the variation in σ_{sp} , σ_{ap} , SAE and AAE is examined against the wind speed and direction
457 (Fig. 9). In general, the results show that the west/southwest flow enhances the scattering and
458 absorption coefficients, while the north air masses are mostly clean. The air flow from southeast
459 direction is mostly associated with the monsoon circulation, higher rainfall and lower aerosol
460 concentrations; however, it was found that the concentrations from this sector are similar to those
461 from southwest during the other seasons. Similar findings (lower values for both scattering and
462 absorption associated with east/southeast directions) were found at Mukteshwar (Hyvarinen et
463 al., 2009), while the highest values were found for western and southwestern sectors. The
464 maximum σ_{sp} and σ_{ap} values are mostly associated with moderate winds (4-6 ms^{-1}), supporting
465 the higher contribution of the transported aerosols at the observational site. In contrast, the
466 accumulation of pollutants over the urban areas is favored by calm winds resulting in larger
467 values of σ_{sp} (almost double for wind speed $< 0.5 \text{ m s}^{-1}$ compared to wind speed $> 3 \text{ m s}^{-1}$) at
468 Anantapur (Gopal et al., 2014). The east flow carries smaller particles with SAE greater than 1.2,
469 which can be up to 1.6-1.8 for certain air masses from southeast; in contrast, the northwest sector
470 is associated with larger particles (much lower values of SAE). However, the AAE is not so
471 much dependent on the wind direction, revealing larger influence by the local emissions as
472 discussed in Fig. 7. The valley-breeze circulation was found to have a strong impact on the
473 aerosol composition even at the high-altitude (5079 m) NCO-P site in the Everest area (Decesari
474 et al., 2010) and, therefore, is considered as the major mechanism for the aerosol transport from
475 the polluted IGP up to Himalayas. This was further supported by chemical analysis of the
476 WIOC/EC (water insoluble organic carbon/elemental carbon) ratios between Nainital and IGP
477 (Ram and Sarin, 2010), which revealed aerosol of similar sources. In synopsis, seasonal changes
478 in meteorology conditions, air-mass origin and transport pathways as well as variations in BLH
479 influence the scattering, absorbing coefficients and their wavelength dependence in Nainital.
480 Various synoptic weather conditions and changes in BLH were also found to play an emerging
481 role in aerosol properties at the high-altitude Jungfraujoch site in Swiss Alps (Collaud Coen et
482 al., 2011).

483
484 The whole analysis revealed that the BLD and LRT play the major role in the aerosol field and
485 temporal evolution over Nainital in all seasons except monsoon, when the rain washout is the
486 main process. The potential aerosol source regions are difficult to be defined by simple air-mass
487 back trajectories or even trajectory clusters. Therefore, an advanced technique (Concentrated
488 Weighted Trajectory, CWT), which is able to quantify the regional contribution of each of

489 advection pathway to the measured aerosol variable (Seibert et al., 1994; Dumka et al., 2013)
 490 was performed by combining statistical analysis of back trajectories with the aerosol properties
 491 (σ_{sp} , σ_{ap} , SAE and AAE). The trajectories ending at 500 m over Nainital were weighted on the
 492 basis of the measured aerosol properties during their arrival and each grid cell is assigned a
 493 concentration obtained by averaging trajectory-associated concentrations that had crossed the
 494 grid cell (Fig. 10 a-d):

$$495 \quad C_{ij} = \frac{1}{\sum_{l=1}^M \tau_{ijl}} \sum_{l=1}^M C_l \tau_{ijl} \quad (1)$$

496 where C_{ij} is the average weighted concentration in a grid cell (i, j), C_l the measured variable, τ_{ijk}
 497 the number of k^{th} trajectory endpoints in the (i, j) grid cell and M the total number of trajectory
 498 endpoints in (i, j) grid (Seibert et al., 1994). The CWT analysis reveals that the major sources
 499 that contribute to the large values of σ_{sp} and σ_{ap} are detected in the northwestern and central IGP,
 500 central and southern Pakistan, arid regions in southwest Asia and, especially for the σ_{ap} (Fig.
 501 10b), eastern IGP, Bangladesh and Bay of Bengal (BoB). It should be noted that the trajectories
 502 from eastern directions mostly occur during monsoon, thus associated with lower σ_{sp} values (Fig.
 503 10a) and higher SAE (Fig. 10c), while the arid regions in the west contribute to lower SAE
 504 values. Finally, the AAE plot (Fig. 10d) clearly differentiates the areas contributing to high
 505 values (southwest arid Asia) from those of moderate-to-low values (central-eastern IGP and
 506 BoB). The former regions contribute to seasonal dust and agricultural burning aerosols
 507 characterized by larger values of AAE compared to the dominance of anthropogenic and fossil-
 508 fuel burning mostly occurred in central-eastern IGP (Ram and Sarin, 2010).

509
 510 Many studies (Eck et al., 2010; Russell et al., 2010; Giles et al., 2012; Vijayakumar et al., 2012;
 511 2014) have suggested the use of correlations between the aerosol absorption and scattering
 512 properties for the discrimination of different aerosol types. In this respect, we correlate the SAE
 513 with AAE for the whole set of measurements for both $D_{1\mu\text{m}}$ and $D_{10\mu\text{m}}$ groups (Fig. 11). Such a
 514 graph is able to reveal the existence of different aerosols, since the wavelength dependence of
 515 scattering and absorption differentiates for the various types. As far as the scattering is
 516 concerned, the fine-mode aerosols (biomass burning, soot, urban/industrial emissions) exhibit
 517 higher values, while sea-salt and desert dust show lower values of SAE. The AAE is commonly
 518 used for aerosol characterization with values around 1 to correspond to vehicle exhausts or fossil
 519 fuel combustions, whereas the AAE values in excess of biomass burning or dust aerosol are

520 around 2 or even more (Kirchstetter et al., 2004; Bergstrom et al., 2007). Using AERONET
521 retrievals, Russell et al. (2010) found AAE values varying between 1.2 and 3.0 for dust, 0.75 and
522 1.3 for urban/industrial, and 1.2 and 2.0 for biomass burning. The range of these values seems to
523 be significant and at the same magnitude (1.2 - 1.8) to those reported by Eck et al. (2010) for
524 mixtures of dust, smoke and pollution. The current results reveal a rather well mixed atmosphere
525 without clear identification of specific aerosol types, as was found over Kanpur during pre-
526 monsoon (TIGERZ campaign, Giles et al., 2011). The SAE and AAE are somewhat
527 homogeneously distributed around the mean values of SAE (0.9-1.1) and AAE (1-1.2), while
528 few cases present large values of SAE associated with AAE of 1.0-1.5 revealing the presence of
529 carbonaceous aerosols of mixed fossil and biofuel combustions. The scatter plot of σ_{sp} vs. σ_{ap}
530 (not shown) exhibited a strong correlation ($R^2 = 0.84$ for both $D_{1\mu m}$ and $D_{10\mu m}$) suggesting
531 covariance in the scattering and absorption properties. For low aerosol loading (i.e., for σ_{sp}
532 values below about 150 Mm^{-1}), the σ_{ap} values are almost similar for $D_{1\mu m}$ and $D_{10\mu m}$ particles
533 suggesting that for clean atmospheres the discrimination of the optical properties between super-
534 micron and sub-micron aerosols is really difficult. Further analysis revealed a general decrease in
535 SAE and AAE with increasing σ_{sp} suggesting an increase in size and ageing aerosol processes
536 (condensation, coagulation) under more turbid atmospheres. These conditions are mostly related
537 to LRT from northwestern IGP and southwest Asia transporting various types of aerosols via
538 upslope flows within a deeper mixing layer.

539

540 4. Conclusions

541 A comprehensive analysis of several extensive and intensive properties (total scattering,
542 backscattering, light absorption and their wavelength dependence) of near-surface aerosols was
543 performed in the current study, aiming to investigate the temporal evolutions and influence of
544 transported plumes and boundary-layer dynamics. The measurements via AMF were performed
545 in Nainital, central Indian Himalayas during June 2011 - March 2012 in the framework of
546 GVAX campaign. More specifically, light scattering and absorption measurements, using three
547 wavelengths integrated Nephelometer and PSAP, respectively were analyzed along with
548 meteorological variables, mixing-layer height and air-mass back trajectories. The main findings
549 of the study are summarized as follows:

550 1. The meteorological field exhibited a seasonal-changing pattern, which along with the
551 boundary layer dynamics and the upslope valley winds control the temporal evolution and the
552 aerosol characteristics at Nainital. The surface wind showed a clear dominance of the
553 northwest (winter and pre-monsoon) and southeast (summer monsoon) directions.

- 554 2. The scattering and absorption coefficients showed higher values during November and March
555 due to the significant influence of biomass-burning aerosols and dust mixed with
556 anthropogenic pollution, respectively, and low values during monsoon due to rainy washout
557 process.
- 558 3. The Ångström wavelength exponents of scattering (SAE) and absorption (AAE) exhibited a
559 seasonal variation, with monsoon high for SAE and late winter-to-March high for AAE. The
560 higher SAE values during monsoon may be related to rainy washout and the removal of the
561 coarser aerosol particles, while a secondary increase of SAE during winter was associated
562 with local emissions from bio-fuel combustion. The latter seems to have an effect in
563 increasing AAE values during the same period, while the higher AAE in March was
564 associated with increased dust occurrence.
- 565 4. The particle size played a major role in the scattering coefficient and SAE, while its effect was
566 much lesser in the absorption processes. Thus, the absorption fraction by the sub-micron
567 particles ($<1 \mu\text{m}$) was about 0.9 of that of $<10 \mu\text{m}$ particles, while the respective scattering
568 fraction was only 0.6.
- 569 5. The diurnal variation of both scattering and absorption coefficients revealed a noon-to-early
570 afternoon maximum, which was clearly defined during October to March, while it was
571 vanished during monsoon. This suggests that the largest aerosol concentrations were mostly
572 attributed to transported plumes from the IGP and southwest Asia and not to local emissions,
573 while the rainy washout effect modulates the diurnal cycle. Furthermore, the diurnal patterns
574 of SAE and AAE revealed slight higher values during early morning and evening hours due to
575 larger influence of the local emissions, suggesting that these aerosols are finer and more
576 absorbing in nature than the aged transported plumes.
- 577 6. The highest values for both scattering and absorption were mostly associated with moderate
578 winds ($3\text{-}5 \text{ ms}^{-1}$) and southwest air flow, suggesting strong influence of transported aerosols
579 from northwestern India and arid southwest Asia, contributing to lower SAE values. The
580 larger influence of the aged transported aerosol plumes controlled by the dynamics in mixing-
581 layer height resulted in a rather well-mixed aerosol field over the site, whereas a specific
582 aerosol type can be detected only in a few cases.

583

584 **Acknowledgement**

585 The authors gratefully acknowledge the NOAA Air Resources Laboratory (ARL) for the
586 provision of the HYSPLIT transport and dispersion model and/or READY website
587 (<http://www.arl.noaa.gov/ready.html>) used in this publication. We are grateful to the US
588 Department of Energy for deploying the Atmospheric Radiation Measurements Climate

589 Research Facility and to the technical staff for providing valuable data
590 (<http://www.archive.arm.gov/>). This study is carried out under GVAX
591 (<https://www.arm.gov/sites/amf/pgh/>) project in collaboration among the DoE, IISc, SPL, ISRO
592 and ARIES. We would like to thank the participants (scientists and technical staff) of the
593 campaign for their valuable help and cooperation. The support from the authorities of all
594 collaborating Institutions involved in the study is acknowledged with thanks. Thanks are also
595 due to the Editor and anonymous reviewers for their insightful comments and valuable
596 suggestions, which improved the scientific content and clarity of the paper.

597

598 **References**

- 599 Adhikary, B., Carmichael G. R., Tang Y., Leung L. R., Qian Y., Schauer J. J., Stone E. A.,
600 Ramanathan V., and Ramana M. V.: Characterization of the seasonal cycle of south Asian
601 aerosols: A regional-scale modeling analysis, *J. Geophys. Res.*, 112, D22S22, doi:
602 10.1029/2006JD008143, 2007.
- 603 Anderson, T. L. and Ogren, J. A.: Determining aerosol radiative properties using the TSI 3563
604 integrating Nephelometer, *Aerosol Sci. Tech.*, 29, 57–69, 1998.
- 605 Anderson, T. L., Covert, D. S., Wheeler, J. D., Harris, J. M., Perry, K. D., Trost, B. E., Jaffe, D.
606 J., and Ogren, J. A.: Aerosol Backscatter Fraction and Single Scattering Albedo: Measured
607 values and uncertainties at a coastal station in the pacific North West, *J. Geophys. Res.*,
608 104(D21), 793–807, 1999.
- 609 Andreae, T.W., Andreae, M.O., Ichoku, C., Maenhaut W., Jan, C., Karnieli, A. and Orlovsky, L.:
610 Light scattering by dust and anthropogenic aerosol at a remote site in the Negev desert, Israel,
611 *J. Geophys. Res.*, 107(D2), 4008, doi: 10.1029/2001JD900252, 2002.
- 612 Andrews, E., Ogren, J.A., Bonasoni, P., Marinoni A., Cuevas E., Rodríguez S., Sun J. Y.,
613 Jaffe D. A., Fischer E.V., Baltensperger U., Weingartner E., Collaud Coen M., Sharma S.,
614 Macdonald A. M., Leitch W. R., Lin N.-H., Laj P., Arsov T. Kalapov I., Jefferson A.,
615 Sheridan P.: Climatology of aerosol radiative properties in the free troposphere, *Atmos. Res.*,
616 102, 365–393, doi:10.1016/j.atmosres.2011.08.017, 2011.
- 617 Antón, M., Valenzuela, A., Cazorla, A., et al.: Global and diffuse shortwave irradiance during a
618 strong desert dust episode at Granada (Spain), *Atmos. Res.*, 118, 232-239, doi:
619 10.1016/j.atmosres.2012.07.007, 2012.
- 620 Beegum S. Naseema, Moorthy K. Krishna, Babu S. Suresh, Satheesh S.K., Vinoj V., Badarinath
621 K.V.S., Safai P.D., Devara P.C.S., Singh Sacchidanand, Vinod, Dumka U. C., Pant P.: Spatial
622 distribution of aerosol black carbon over India during pre-monsoon Season, *Atmos. Environ.*,
623 43, 1071–1078, doi:10.1016/j.atmosenv.2008.11.042, 2009.
- 624 Bergstrom, R. W., Pilewskie, P., Russell, P. B., Redemann, J., Bond, T. C., Quinn, P. K., and
625 Sierau, B.: Spectral absorption properties of atmospheric aerosols, *Atmos. Chem. Phys.*, 7,
626 5937–5943, 2007, <http://www.atmos-chem-phys.net/7/5937/2007/>.
- 627 Bollasina M., and Nigam S.: Absorbing aerosols and pre-summer monsoon hydroclimate
628 variability over the Indian subcontinent: The challenge in investigating links, *Atmos. Res.*, 94,
629 338–344, doi:10.1016/j.atmosres.2009.06.008, 2009.

630 Bond, T. C., Anderson, T. L., and Campbell, D.: Calibration and intercomparison of filter-based
631 measurements of visible light absorption by aerosols, *Aerosol Sci. Tech.*, 30, 582–600, 1999.
632 Bond, T. C.: Spectral dependence of visible light absorption by carbonaceous particles emitted
633 from coal combustion, *Geophys. Res. Lett.*, 28, 4075–4078, 2001.
634 Boss, E., Pegau W. S., Lee M., Twardowski M., Shybanov E., Korotaev G., and Baratange F.:
635 Particulate backscattering ratio at LEO 15 and its use to study particle composition and
636 distribution, *J. Geophys. Res.*, 109, C01014, doi: 10.1029/2002JC001514, 2004.
637 Bucci, S., Cagnazzo C., Cairo F., Di Liberto L., and Fierli, F: Aerosol variability and
638 atmospheric transport in the Himalayan region from CALIOP 2007–2010 observations,
639 *Atmos. Chem. Phys.*, 14, 4369–4381, doi:10.5194/acp-14-4369-2014, 2014.
640 Carrico, C. M., Kus P., Rood M. J., Quinn P. K., and Bates T. S.: Mixtures of pollution, dust, sea
641 salt, and volcanic aerosol during ACE-Asia: Radiative properties as a function of relative
642 humidity, *J. Geophys. Res.*, 108(D23), 8650, doi: 10.1029/2003JD003405, 2003.
643 Collaud Coen, M., Weingartner, E., Schaub, D., Hueglin, C., Cor rigan, C., Henning, S.,
644 Schwikowski, M., and Baltensperger, U.: Saharan dust events at the Jungfraujoch: detection
645 by wavelength dependence of the single scattering albedo and first climatology analysis,
646 *Atmos. Chem. Phys.*, 4, 2465–2480, doi:10.5194/acp 4-2465-2004, 2004.
647 Collaud Coen, M., Weingartner, E., Furger, M., Nyeki, S., Prévôt, A. S. H., Steinbacher, M., and
648 Baltensperger, U.: Aerosol climatology and planetary boundary influence at the Jungfraujoch
649 analyzed by synoptic weather types, *Atmos. Chem. Phys.*, 11, 5931–5944, doi:10.5194/acp-
650 11-5931-2011, 2011.
651 Decesari S, Facchini M.C, Carbone C, Giulianelli L, Rinaldi M, Finessi E, et al.: Chemical
652 composition of PM₁₀ and PM₁ at the high-altitude Himalayan station Nepal Climate
653 Observatory-Pyramid (NCO-P) (5079 m a.s.l.), *Atmos. Chem. Phys.*, 10, 4583-4596,
654 doi:10.5194/acp-10-4583-2010, 2010.
655 Di Girolamo, L., Bond T. C., Bramer D., Diner D. J., Fettinger F., Kahn R. A., Martonchik J. V.,
656 Ramana M. V., Ramanathan V., and Rasch P. J.: Analysis of Multi-angle Imaging
657 Spectroradiometer (MISR) aerosol optical depths over greater India during winter 2001–2004,
658 *Geophys. Res. Lett.*, 31, L23115, doi: 10.1029/2004GL021273, 2004.
659 Dipu, S., Prabha Thara V., Pandithurai G., Dudhia J., Pfister G., Rajesh K., and Goswami B.N.:
660 Impact of elevated aerosol layer on the cloud macrophysical properties prior to monsoon
661 onset, *Atmos. Environ.*, 70, 454-467, 2013.
662 Doherty, S. J., Quinn P. K., Jefferson A., Carrico C. M., Anderson T. L. and Hegg D.: A
663 comparison and summary of aerosol optical properties as observed in situ from aircraft, ship,
664 and land during ACE-Asia, *J. Geophys. Res.*, 110, D04201, doi: 10.1029/2004JD004964,
665 2005.
666 Draxler, R. et al.: HYSPLIT4 user's guide, version 4, report, NOAA, Silver Spring, Md.
667 [www.arl.noaa.gov/documents/reports/hysplit_user_guide.pdf], 2012.
668 Dumka U. C., Moorthy K Krishna, Satheesh S. K., Sagar Ram and Pant P.: Short-Period
669 Modulations in Aerosol Optical Depths over the Central Himalayas: Role of Mesoscale
670 Processes, *J. Appl. Meteorol. Climatol*, 47, 1467-1475, DOI: 10.1175/2007JAMC1638.1,
671 2008.
672 Dumka, U. C. and Kaskaoutis D. G.: In-situ measurements of aerosol properties and estimates of
673 radiative forcing efficiency over Gangetic-Himalayan region during the GVAX field
674 campaign, *Atmos. Environ.*, 94, 96-105, 10.1016/j.atmosenv.2014.05.021, 2014.

675 Dumka, U. C., Satheesh S. K., Pant P., Hegde P. and Moorthy K. Krishna: Surface changes in
676 solar irradiance due to aerosols over central Himalayas, *Geophys. Res. Lett.*, 33, L20809, doi:
677 10.1029/2006GL027814, 2006.

678 Dumka, U.C., Moorthy K. K., Kumar, R., Hegde, P., Sagar, R., Pant, P., Singh, N., and Babu, S.
679 S.: Characteristics of aerosol black carbon mass concentration over a high altitude location in
680 the Central Himalayas from multi-year measurements, *Atmos. Res.*, 96, 4, 510–521,
681 doi:10.1016/j.atmosres.2009.12.010, 2010.

682 Dumka, U.C., Manchanda, R.K., Sinha, P.R., Sreenivasan, S., Moorthy, K.K., and Babu, S.S.:
683 Temporal variability and radiative impact of Black Carbon aerosol over tropical urban station
684 Hyderabad, *J. Atmos. Sol-Terr. Phys.*, 105–106, 81-90, 2013.

685 Dumka, U.C., Bhattu, D., Tripathi, S.N., Kaskaoutis, D.G., and Madhavan, B.L.: Seasonal
686 inhomogeneity in cloud precursors over Gangetic Himalayan region during GVAX campaign,
687 *Atmos. Res.*, 155, 158-175, doi:10.1016/j.atmosres.2014.11.022, 2015.

688 Eck, T. F., Holben B. N., Sinyuk A., Pinker R. T., Goloub P., Chen H., Chatenet B., Li Z., Singh
689 R. P., Tripathi S. N., Reid J. S., Giles D. M., Dubovik O., O'Neill N. T., Smirnov A., Wang P.
690 and Xia X.: Climatological aspects of the optical properties of fine/coarse mode aerosol
691 mixtures, *J. Geophys. Res.*, 115, D19205, doi: 10.1029/2010JD014002, 2010.

692 Fierz-Schmidhauser R., Zieger P., Gysel M., Kammermann L., DeCarlo P. F., Baltensperger U.,
693 and Weingartner E.: Measured and predicted aerosol light scattering enhancement factors at
694 the high alpine site Jungfraujoch, *Atmos. Chem. Phys.*, 10, 2319–2333, 2010.

695 Formenti P., Andreae M. O., Andreae T. W., Ichoku C., Schebeske G., Kettle J., Maenhaut W.
696 Cafmeyer J., Ptasinaky J., Karnieli A. and Lelieveld J.: Physical and chemical characteristics
697 of aerosols over the Negev Desert (Israel) during summer 1996, *J. Geophys. Res.*,
698 106(D5), 4871-4890, 2001.

699 Ganguly, D., Jayaraman A., Rajesh T. A., and Gadhavi H: Wintertime aerosol properties during
700 foggy and non foggy days over urban center Delhi and their implications for shortwave
701 radiative forcing, *J. Geophys. Res.*, 111, D15217, doi: 10.1029/2005JD007029, 2006.

702 Ganguly, D., Rasch P. J., Wang H., and Yoon J.H.: Climate response of the South Asian
703 monsoon system to anthropogenic aerosols. *J. Geophys. Res.*, 117, D13209, doi:
704 10.1029/2012JD017508, 2012.

705 Gautam R., Hsu N. C., Tsay S. C., Lau K. M., Holben B., Bell S., Smirnov A., Li C., Hansell R.,
706 Ji Q., Payra S., Aryal D., Kayastha R. and Kim K. M.: Accumulation of aerosols over the
707 Indo-Gangetic plains and southern slopes of the Himalayas: distribution, properties and
708 radiative effects during the 2009 pre-monsoon season, *Atmos. Chem. Phys.*, 11, 12841–
709 12863, doi: 10.5194/acp-11-12841-2011, 2011.

710 Gautam, R., Hsu, N. C., and Lau, K.-M.: Premonsoon aerosol characterization and radiative
711 effects over the Indo-Gangetic Plains: Implications for regional climate warming, *J. Geophys.*
712 *Res.*, 115, D17208, doi: 10.1029/2010JD013819, 2010.

713 Giles DM, Holben BN, Tripathi SN, Eck T, Newcomb W, Slutsker I, Dickerson R, Thompson A,
714 Mattoo S, Wang S, Singh R, Sinyuk A, Schafer J (2011). Aerosol Properties over the Indo-
715 Gangetic Plain: A 1 Mesoscale Perspective from the TIGERZ Experiment. *J Geophys Res*
716 116: D18203, doi: 10.1029/2011JD015809

717 Giles, D. M., Holben B. N., Eck T. F., Sinyuk A., Smirnov A., Slutsker I., Dickerson R. R.,
718 Thompson A. M., and Schafer J. S.: An analysis of AERONET aerosol absorption properties

719 and classifications representative of aerosol source regions, *J. Geophys. Res.*, 117, D17203,
720 doi: 10.1029/2012JD018127, 2012.

721 Gopal K. Rama, Arafath S. Md., Lingaswamy A.P., Balakrishnaiah G., Kumari S. Pavan, Uma
722 Devi K., Reddy N. Siva Kumar, Reddy K. Raja Obul, Reddy M. Penchal, Reddy R.R., Babu
723 S. Suresh: In-situ measurements of atmospheric aerosols by using Integrating Nephelometer
724 over a semi-arid station, southern India, *Atmos. Environ.*, 86, 228-240, 2014.

725 Guleria Raj Paul, Kuniyal Jagdish Chandra, Rawat Pan Singh, Sharma Nand Lal, Thakur
726 Harinder Kumar, Dhyani Pitamber Prasad and Singh Mahavir: The assessment of aerosol
727 optical properties over Mohal in the northwestern Indian Himalayas using satellite and
728 ground-based measurements and an influence of aerosol transport on aerosol radiative
729 forcing, *Meteorol Atmos Phys*, 113, 153-169, DOI 10.1007/s00703-011-0149-5, 2011.

730 Hegde P. and Kawamura K.: Seasonal variations of water-soluble organic carbon, dicarboxylic
731 acids, ketocarboxylic acids, and α -dicarbonyls in Central Himalayan aerosols, *Atmos. Chem.*
732 *Phys.*, 12, 6645–6665, doi: 10.5194/acp-12-6645-2012, 2012.

733 Hegde, P., Pant, P., Naja, M., Dumka, U. C., and Sagar, R.: South Asian dust episode in June
734 2006: Aerosol observations in the central Himalayas, *Geophys. Res. Lett.*, 34, L23802, doi:
735 10.1029/2007GL030692, 2007.

736 Heintzenberg, J., Wiedensohler, A., Tuch, T. M., Covert, D. S., Sheridan, P., Ogren, J. A., Gras,
737 J., Nessler, R., Kleefeld, C., Kalivitis, N., Aaltonen V., Wilhelm, R. T., and Havlicek, M.:
738 Intercomparison and aerosol calibrations of 12 commercial integrating Nephelometer of three
739 manufacturers, *J. Atmos. Ocean. Tech.*, 23, 902–914, 2006.

740 Hyvärinen A.-P., Raatikainen T., Brus D., Komppula M., Panwar T. S., Hooda R. K., Sharma V.
741 P., and Lihavainen H.: Effect of the summer monsoon on aerosols at two measurements
742 stations in Northern India – Part 1: PM and BC concentrations, *Atmos. Chem. Phys.*, 11,
743 8271–8282, doi:10.5194/acp-11-8271-2011, 2011a.

744 Hyvärinen A.-P., Raatikainen T., Komppula M., Mielonen T., Sundström A.-M., Brus D.,
745 Panwar T. S., Hooda R. K., Sharma V. P., de Leeuw G., and Lihavainen H.: Effect of the
746 summer monsoon on aerosols at two measurement stations in Northern India – Part 2:
747 Physical and optical properties, *Atmos. Chem. Phys.*, 11, 8283–8294, doi: 10.5194/acp-11-
748 8283-2011, 2011b.

749 Hyvärinen, A.-P., Lihavainen, H., Komppula, M., Sharma, V. P., Kerminen, V.-M., Panwar, T.
750 S., and Viisanen, Y.: Continuous measurements of optical properties of atmospheric aerosols
751 in Mukteshwar, Northern India, *J. Geophys. Res.*, 114, D08207, doi: 10.1029/2008JD011489,
752 2009.

753 Jayaraman A., Gadhavi H., Misra A., Ganguly D., Ramachandran S. and Rajesh T.A.: Spatial
754 variations in aerosol characteristics and regional radiative forcing over India: Measurements
755 and modeling of 2004 road campaign experiment, *Atmos. Environ.*, 40, 6504–6515,
756 doi:10.1016/j.atmosenv.2006.01.034, 2006.

757 Jefferson A.: Aerosol Observing System (AOS) Handbook, DOE/SC-ARM/TR-014,
758 http://www.arm.gov/publications/tech_reports/handbooks/aos_handbook.pdf, 2011.

759 Kaskaoutis D. G., Singh Ramesh P, Gautam Ritesh, Sharma Manish, Kosmopoulos P G and
760 Tripathi S N.: Variability and trends of aerosol properties over Kanpur, northern India using
761 AERONET data (2001-10), *Environ. Res. Lett.*, 7, 024003, doi:10.1088/1748-
762 9326/7/2/024003, 2012.

763 Kaskaoutis D.G., Kumar S., Sharma D., Singh R.P., Kharol S.K., Sharma M., Singh A.K., Singh
764 S., Singh Atinderpal and Singh D.: Effects of crop residue burning on aerosol properties,
765 plume characteristics and longrange transport over northern India, *J. Geophys. Res.*, doi:
766 10.1002/2013JD021357, 2014.

767 Kaskaoutis D.G., Sinha P.R., Vinoj V., Kosmopoulos P. G., Tripathi S. N., Misra Amit, Sharmaf
768 M., Singh R. P.: Aerosol properties and radiative forcing over Kanpur during severe aerosol
769 loading conditions, *Atmos. Environ.*, 79, 7-19, doi:10.1016/j.atmosenv.2013.06.020, 2013.

770 Kirchstetter, T. W., Novakov T., and Hobbs P. V.: Evidence that the spectral dependence of light
771 absorption by aerosols is affected by organic carbon, *J. Geophys. Res.*, 109, D21208, doi:
772 10.1029/2004JD004999, 2004.

773 Komppula, M., Lihavainen, H., Hyvärinen, A.-P., Kerminen, V.-M., Panwar, T. S., Sharma, V.
774 P., and Viisanen, Y.: Physical properties of aerosol particles at a Himalayan background site
775 in India, *J. Geophys. Res.*, 114, D12202, doi: 10.1029/2008JD011007, 2009.

776 Kopacz, M., Jacob, D. J., Fisher, J. A., Logan, J. A., Zhang, L., Megretskaia, I. A., Yantosca, R.
777 M., Singh, K., Henze, D. K., Burrows, J. P., Buchwitz, M., Khlystova, I., McMillan, W. W.,
778 Gille, J. C., Edwards, D. P., Eldering, A., Thouret, V., and Nedelec, P.: Global estimates of
779 CO sources with high resolution by adjoint inversion of multiple satellite datasets (MOPITT,
780 AIRS, SCIAMACHY, TES), *Atmos. Chem. Phys.*, 10, 855–876, doi:10.5194/acp-10-855-
781 2010, 2010.

782 Kotamarthi, V. R. and Satheesh S. K.: Ganges Valley Aerosol Experiment, Air & Waste
783 Management Association, Em, The magazine for environmental managers, 2011.

784 Kumar, R., Barth M. C., Pfister G. G., Naja M. and Brasseur G. P.: WRF-Chem simulations of a
785 typical pre-monsoon dust storm in northern India: influences on aerosol optical properties and
786 radiation budget, *Atmos. Chem. Phys.*, 14, 2431–2446, doi: 10.5194/acp-14-2431-2014, 2014.

787 Lau K M, Kim M K, Kim K M.: Asian summer monsoon anomalies induced by aerosol direct
788 forcing: the role of the Tibetan Plateau, *Clim Dyn.*, 26, 855–864, DOI 10.1007/s00382-014-
789 2055-2, 2006.

790 Lawrence, M. G. and Lelieveld, J.: Atmospheric pollutant outflow from Southern Asia: a review,
791 *Atmos. Chem. Phys.*, 10, 11017-11096, doi: 10.5194/acp-10-11017-2010, 2010.

792 León, J.-F., and Legrand M.: Mineral dust sources in the surroundings of the north Indian Ocean,
793 *Geophys. Res. Lett.*, 30(6), 1309, doi: 10.1029/2002GL016690, 2003.

794 Liu Z., Liu D., Huang J., Vaughan M., Uno I., Sugimoto N., Kittaka C., Trepte C., Wang Z.,
795 Hostetler C., and Winker D.: Airborne dust distributions over the Tibetan Plateau and
796 surrounding areas derived from the first year of CALIPSO lidar observations, *Atmos. Chem.*
797 *Phys.*, 8, 5045–5060, 2008.

798 Lu, Z, Zhang Q., and Streets D.G.: Sulfur dioxide and primary carbonaceous aerosol emissions
799 in China and India, 1996–2010, *Atmos. Chem. Phys.*, 11, 9839-9864, doi: 10.5194/acp-11-
800 9839-2011, 2011.

801 Manoharan V. S., Kotamarthi R., Feng Y., and Cadeddu M. P.: Increased absorption by coarse
802 aerosol particles over the Gangetic–Himalayan region, *Atmos. Chem. Phys.*, 14, 1159–1165,
803 doi: 10.5194/acp-14-1159-2014, 2014.

804 Manoj M. G., Devara, P. C. S., Safai P. D., and Goswami B. N.: Absorbing aerosols facilitate
805 transition of Indian monsoon breaks to active spells, *Clim Dyn* 37, 2181-2198, 2011.

806 Marcq, S., Laj, P., Roger, J. C., Villani, P., Sellegri, K., Bonasoni, P., Marinoni, A., Cristofanelli,
807 P., Verza, G. P., and Bergin, M.: Aerosol optical properties and radiative forcing in the high

808 Himalaya based on measurements at the Nepal Climate Observatory-Pyramid site (5079 m
809 a.s.l.), *Atmos. Chem. Phys.*, 10, 5859–5872, doi:10.5194/acp-10-5859-2010, 2010.

810 Marinoni, A., Cristofanelli, P., Laj, P., Duchi, R., Calzolari, F., Decesari, S., et al.: Aerosol mass
811 and black carbon concentrations, a two year record at NCO-P (5079 m, Southern Himalayas),
812 *Atmos. Chem. Phys.*, 10, 8551-8562, doi: 10.5194/acp-10-8551-2010, 2010.

813 Nakajima, T., Yoon, S.-C., Ramanathan, V., Shi, G.-Y., Takemura, T., Higurashi, A., Takamura,
814 T., Aoki, K., Sohn, B.-J., Kim, S.-W., Tsuruta, H., Sugimoto, N., Shimizu, A. Tanimoto, H.,
815 Sawa, Y., Lin, N.-H., Lee, C.-T., Goto, D., and Schutgens, N.: Overview of the atmospheric
816 Brown Cloud East Asian Regional Experiment 2005 and a study of the aerosol direct radiative
817 forcing in east Asia, *J. Geophys. Res.*, 112, D24S91, doi: 10.1029/2007JD009009, 2007.

818 Neitola K., Asmi E., Komppula M., Hyvärinen A.-P. Raatikainen T., Panwar T. S., Sharma V. P.
819 and Lihavainen H.: New particle formation infrequently observed in Himalayan foothills –
820 why?, *Atmos. Chem. Phys.*, 11, 8447–8458, doi: 10.5194/acp-11-8447-2011, 2011.

821 Ogren, J.A.: Comment on “Calibration and Intercomparison of Filter-Based Measurements of
822 Visible Light Absorption by Aerosols”, *Aerosol Sci. Tech.*, 44, 589–591, 2010.

823 Pandolfi, M., Ripoll, A., Querol, X., and Alastuey, A.: Climatology of aerosol optical properties
824 and black carbon mass absorption cross section at a remote high-altitude site in the western
825 Mediterranean Basin, *Atmos. Chem. Phys.*, 14, 6443-6460, doi:10.5194/acp-14-6443-2014,
826 2014.

827 Pant, P., Hegde, P., Dumka, U. C., Sagar, R., Satheesh, S. K., Moorthy, K. K., Saha, A., and
828 Srivastava, M. K.: Aerosol characteristics at a high-altitude location in central Himalayas:
829 Optical properties and radiative forcing, *J. Geophys. Res.*, 111, D17206, doi:
830 10.1029/2005JD006768, 2006.

831 Panwar T. S., Hooda Rakesh K., Lihavainen H., Hyvärinen A. P., Sharma V. P., Viisanen Y.:
832 Atmospheric aerosols at a regional background Himalayan site-Mukteshwar, India, *Environ*
833 *Monit Assess*, 185:4753–4764, DOI 10.1007/s10661-012-2902-8, 2013.

834 Pathak, B., Bhuyan, P.K., Biswas, J., and Takemura, T.: Long term climatology of Particulate
835 Matter and associated microphysical and optical properties over Dibrugarh, North-East India
836 and inter-comparison with SPRINTARS simulations, *Atmos. Environ.*, 69, 334-344, 2013.

837 Prabha T. V., Karipot, A., Axisa D., Padmakumari B., Maheskumar R. S., Konwar M., Kulkarni
838 J. R., Goswami B. N.: Scale interactions near the foothills of Himalaya during CAIPEEX, *J.*
839 *Geophys. Res.*, 117, D10203, 495 doi: 10.1029/2011JD0167, 2012.

840 Raatikainen T., Hyvärinen A.-P., Hatakka J., Panwar T.S., Hooda R.K., Sharma V.P., Lihavainen
841 H.: The effect of boundary layer dynamics on aerosol properties at the Indo-Gangetic plains
842 and at the foothills of the Himalayas, *Atmos. Environ.*, 89, 548-555,
843 <http://dx.doi.org/10.1016/j.atmosenv.2014.02.058>, 2014.

844 Ram Kirpa and Sarin M. M: Spatio-temporal variability in atmospheric abundances of EC, OC
845 and WSOC over Northern India, *J. Aer. Sci.*, 41(1), 88-98,
846 doi:10.1016/j.jaerosci.2009.11.004, 2010.

847 Ram, K., Sarin, M. M., and Hedge, P.: Atmospheric abundances of primary and secondary
848 carbonaceous species at two high-altitude sites in India: Sources and temporal variability,
849 *Atmos. Environ.*, 42(28), 6785–6796, 2008.

850 Ram, K., Sarin, M. M., and Tripathi, S. N.: A 1 year record of carbonaceous aerosols from an
851 urban site in the Indo-Gangetic Plain: Characterization, sources, and temporal variability, *J.*
852 *Geophys. Res.*, 115, D24313, doi: 10.1029/2010JD014188, 2010.

853 Ramanathan, V., Chung, C., Kim, D., Bettge, T., Buja, L., Kiehl, J.T., Washington, W.M., Fu,
854 Q., Sikka, D.R., Wild, M.: Atmospheric brown clouds: impacts on South Asian climate and
855 hydrological cycle. *PNAS* 102 (15), 5326-5333. <http://dx.doi.org/10.1073/pnas.0500656102>,
856 2005.

857 Ramanathan, V., Li F., Ramana M. V., Praveen P. S., Kim D., Corrigan C. E., Nguyen H., Stone
858 Elizabeth A., Schauer James J., Carmichael, G. R. Adhikary Bhupesh, and Yoon S. C.:
859 Atmospheric brown clouds: Hemispherical and regional variations in long-range transport,
860 absorption, and radiative forcing, *J. Geophys. Res.*, 112, D22S21, doi:
861 10.1029/2006JD008124, 2007.

862 Randles, C. A. and Ramaswamy, V.: Absorbing aerosols over Asia: A Geophysical Fluid
863 Dynamics Laboratory general circulation model sensitivity study of model response to aerosol
864 optical depth and aerosol absorption, *J. Geophys. Res.*, 113, D21203, doi:
865 10.1029/2008JD010140, 2008.

866 Russell, P. B., Bergstrom R. W., Shinozuka Y., Clarke A. D., DeCarlo P. F., Jimenez J. L.,
867 Livingston J. M., Redemann J., Dubovik O., and Strawa A.: Absorption Ångström Exponent
868 in AERONET and related data as an indicator of aerosol composition, *Atmos. Chem. Phys.*,
869 10, 1155–1169, doi:10.5194/acp-10-1155-2010, 2010.

870 Sarkar, C., Chatterjee, A., Singh, A.K., Ghosh, S.K., and Raha, S.: Characterization of Black
871 Carbon aerosols over Darjeeling - A high altitude Himalayan station in Eastern India, *Aeros.*
872 *Air Qual. Res.*, (in press), doi: 10.4209/aaqr.2014.02.0028, 2014.

873 Seibert P, et al.: Trajectory analysis of aerosol measurements at high alpine sites, in *Transport*
874 *and Transformation of Pollutants in the Troposphere: Proceedings of EUROTRAC*
875 *Symposium '94*. Edited by Borrell PM Cvitas T, Seiler W, pp. 689– 693, SPB Acad. Publ.,
876 Hague, The Netherlands, 1994.

877 Sheridan, P. J. and Ogren, J. A.: Observations of the vertical and regional variability of aerosol
878 optical properties over central and eastern North America, *J. Geophys. Res.*, 104, 16793–
879 16805, doi: 10.1029/1999JD900241, 1999.

880 Sheridan, P. J., Delene, D. J., and Ogren, J. A.: Four years of continuous surface aerosol
881 measurements from the Department of Energy's Atmospheric Radiation Measurement
882 Program Southern Great Plains Cloud and Radiation Testbed site, *J. Geophys. Res.*, 106,
883 20735–20747, doi: 10.1029/2001JD000785, 2001.

884 Srivastava, A.K., Singh, S., Pant, P., and Dumka, U.C.: Characteristics of Black Carbon over
885 Delhi and Manora Peak – a comparative study, *Atmos. Sci. Lett.* 13, 223-230, 2012.

886 Titos, G., Jefferson, A., Sheridan, P. J., Andrews, E., Lyamani, H., Alados-Arboledas L., and
887 Ogren J. A.: Aerosol light-scattering enhancement due to water uptake during TCAP
888 campaign, *Atmos. Chem. Phys.*, 14, 7031–7043, doi: 10.5194/acp-14-7031-2014, 2014a.

889 Titos, G., Lyamani, H., Cazorla, A., Sorribas, M., Foyo-Moreno, I., Wiedensohler, A. and
890 Alados-Arboledas, L.: Study of the relative humidity dependence of aerosol light-scattering in
891 southern Spain, *Tellus B*, 66, 24536, <http://dx.doi.org/10.3402/tellusb.v66.24536>, 2014b.

892 Twardowski Michael S., Boss Emmanuel, Macdonald Jacob B., Pegau W. Scott, Barnard
893 Andrew H., and Zaneveld J. Ronald V.: A model for estimating bulk refractive index from the
894 optical backscattering ratio and the implications for understanding particle composition in
895 case I and case II waters, *J. Geophys. Res.*, 106, 14,129-14,142, 2001.

896 Vijayakumar, K., Devara, P.C.S. and Sonbawne, S.M.: Type-segregated aerosol effects on
897 regional monsoon activity: A study using ground-based experiments and model simulations,
898 *Atmos. Environ.*, **99**, 650-659, 2014.

899 Vijayakumar, K., Devara P.C.S., and Simha, C.P.: Aerosol features during drought and normal
900 monsoon years: A study undertaken with multi-platform measurements over a tropical urban
901 site, *Aero. Air Qual. Res.*, **12**, 1444-1458, 2012.

902 Virkkula A., Backman J., Aalto P. P., Hulkkonen M., Riuttanen L., Nieminen T., dal Maso M.,
903 Sogacheva L., de Leeuw G., and Kulmala M.: Seasonal cycle, size dependencies, and source
904 analyses of aerosol optical properties at the SMEAR II measurement station in Hyytiälä,
905 Finland, *Atmos. Chem. Phys.*, **11**, 4445–4468, doi:10.5194/acp-11-4445-2011, 2011.

906 Xu, C., Ma Y. M., Pandey A., Cong Z. Y., Yang K., Zhu Z. K., Wang J. M., Amatya P. M., and
907 Zhao L: Similarities and differences of aerosol optical properties between southern and
908 northern slopes of the Himalayas, *Atmos. Chem. Phys.*, **14**, 3133–3149, doi: 10.5194/acp-14-
909 3133-2014, 2014.

910

911 **Table 1:** Details of AOS instruments, variables and equations used for the calculation of aerosol optical properties.

Instruments	Primary measurements	Derived variables	Equation
Three wavelength Nephelometer (TSI Model 3563)	Total scattering and hemispheric backscattering coefficients (σ_{sp} & σ_{bsp}) from D_1 and D_{10} particles at blue (0.45), green (0.55) and red (0.70) μm	Hemispheric backscatter fraction Scattering Ångström exponent Backscattering Ångström exponent Submicron scattering fraction	$b = \sigma_{bsp}/\sigma_{sp}$ $SAE = -\log[\sigma_{sp}(\lambda_1)/\sigma_{sp}(\lambda_2)]/\log[\lambda_1/\lambda_2]$ $BAE = -\log[\sigma_{bsp}(\lambda_1)/\sigma_{bsp}(\lambda_2)]/\log[\lambda_1/\lambda_2]$ $R_{sp} = \sigma_{sp}(D_1)/\sigma_{sp}(D_{10})$
Radiance Research Particle Soot Absorption Photometer (PSAP)	Light absorption coefficient (σ_{ap}) from D_1 and D_{10} particles at blue (0.467), green (0.53) and red (0.66) μm	Absorption Ångström exponent Submicron absorption fraction	$AAE = -\log[\sigma_{ap}(\lambda_1)/\sigma_{ap}(\lambda_2)]/\log[\lambda_1/\lambda_2]$ $R_{ap} = \sigma_{ap}(D_1)/\sigma_{ap}(D_{10})$

912
913
914
915
916
917
918
919
920
921
922
923
924

925 **Table 2:** Summary of the extensive and intensive aerosol properties during the GVAX campaign (June 2011 – March 2012). The
 926 values in parenthesis refer to the $D_{1\mu\text{m}}$ particles.

Parameter	Winter (Dec-Feb)	Pre-monsoon (Mar)	Monsoon (Jun-Sep)	Post-monsoon (Oct-Nov)	Whole period (Jun 11–Mar 12)
σ_{sp} (Mm^{-1}) [0.55 μm]	185.29 ± 73.46 (122.70±51.39)	228.95 ± 65.00 (122.26 ± 40.01)	113.87 ± 08.58 (53.97 ± 5.28)	282.43 ± 103.25 (158.87 ± 61.88)	177.2 ± 157.5 (104.4±94.2)
σ_{bsp} (Mm^{-1}) [0.55 μm]	13.27 ± 5.73 (9.58 ± 3.93)	19.47 ± 6.18 (11.83 ± 3.30)	7.46 ± 5.89 (4.09 ± 2.65)	19.43 ± 9.77 (12.10 ± 5.78)	12.58 ± 11.46 (8.18±7.39)
σ_{ap} (Mm^{-1}) [0.53 μm]	11.15 ± 6.71 (9.20 ± 5.73)	13.89 ± 9.37 (10.41 ± 7.27)	6.21 ± 1.37 (5.20 ± 1.30)	16.07 ± 7.43 (12.17 ± 5.66)	13.49 ± 13.02 (8.95±8.28)
SAE [0.45/0.70 μm]	0.75 ± 0.05 (1.19 ± 0.05)	0.44 ± 0.05 (0.95 ± 0.05)	0.91 ± 0.02 (1.42 ± 0.02)	0.55 ± 0.04 (1.02 ± 0.04)	0.72 ± 0.42 (1.21 ± 0.35)
BAE [0.45/0.70 μm]	0.31 ± 0.14 (0.49 ± 0.13)	0.10 ± 0.15 (0.34 ± 0.17)	0.26 ± 0.26 (0.45 ± 0.22)	0.13 ± 0.11 (0.31 ± 0.09)	0.24 ± 0.21 (0.42 ± 0.18)
AAE [0.47/0.66 μm]	1.25 ± 0.07 (1.29 ± 0.04)	1.27 ± 0.09 (1.34 ± 0.08)	0.93 ± 0.05 (0.96± 0.04)	1.11 ± 0.08 (1.22 ± 0.04)	1.07 ± 0.20 (1.14 ± 0.18)
b [0.55 μm]	0.072 ± 0.012 (0.083 ± 0.014)	0.084 ± 0.001 (0.096 ± 0.011)	0.057 ± 0.012 (0.063 ± 0.012)	0.069 ± 0.013 (0.077 ± 0.001)	0.067 ± 0.009 (0.073 ± 0.012)
R _{sp} [0.55 μm]	0.67 ± 0.08	0.54 ± 0.08	0.60 ± 0.18	0.58 ± 0.09	0.61 ± 0.13
R _{ap} [0.53 μm]	0.83 ± 0.07	0.75 ± 0.07	0.88 ± 0.11	0.77 ± 0.09	0.83 ± 0.11

927

928

929

930

931

932 **Table 3:** Comparison of extensive and intensive aerosol properties over Nainital during GVAX campaign along with those measured
 933 over mountainous or remote areas over the globe.

Sampling Site	Elevation (m)	Sampling Period	σ_{sp} (Mm ⁻¹)	σ_{ap} (Mm ⁻¹)	SAE	AAE	Reference
Nainital	1958	Jun-11-Mar-12	177.20 (104.40)*	13.49 (8.95)*	0.72 (1.21)*	1.07 (1.14)*	Present study
Nainital	1958	Feb-05 – Jul-08	--	13.9	--	--	Ram et al. (2010)
Nainital	1958	Dec-04	--	12.9	--	--	Ram and Sarin (2009)
Nainital	1958	Feb-05 - Jun-07	--	12.2	--	--	Ram and Sarin (2009)
Mukteshwar	2180	Sep-05 – Sep-07	53.00	11.00	--	1.0 - 1.6	Hyvärinen et al. (2009)
Mukteshwar	2180	2006 to 2009	34.30 – 133.80	6.90 – 25.8	--	--	Hyvärinen et al. (2011b)
NCO-P	5079	May - Sep-06	--	1.1	--	--	Marcq et al. (2010)
Mt. Abu	1700	Dec-05 - Feb-06	--	8.0	--	--	Ram and Sarin (2009)
Mt. Abu	1700	May-05 -Feb-06	--	5.8	--	--	Ram and Sarin (2009)
Jungfrauoch, Swiss Alps	3580	5-11 May 2001	~2-11	~0.2-8	~0.5-2.2	~0.9 - 2.1	Collaud Coen et al. (2004)
Jungfrauoch,S wiss Alps	3580	May 2008**	11.9	--	1.79	--	Fierz-Schmidhauser et al.(2010)
		May 2008****	20.5	--	1.67	--	Fierz-Schmidhauser et al.(2010)
Mauna Loa, USA	3400	^a 2000-2009	1.92(1.24)	0.07(0.07)	1.53(1.35)	--	Andrews et al. (2011)
Whistler Canada	2200	^b 2008-2009	3.98(3.95)	0.54(0.53)	2.01(2.01)	--	Andrews et al. (2011)
Mount Bachelor, USA	2800	^c April-May, 2008-2009	5.32(3.50)	1.00(0.77)	2.54(2.50)	--	Andrews et al. (2011)
Southern Great Plains		^d 2000-2007	13.00(5.73)	0.77(0.49)	2.09(1.89)	--	Andrews et al. (2011)
Bondville		^e 2006-2009	15.30(4.89)	1.00(0.31)	1.91(1.38)	--	Andrews et al. (2011)
Izana, Spain	2400	^a 2008-2009	9.32(6.57)	0.71(0.43)	0.73(0.63)	--	Andrews et al. (2011)
Jungfrauoch, Switzerland	3600	^e 1995-2007	3.50(5.87)	0.50(0.42)	1.85(1.75)	--	Andrews et al. (2011)

Monte Cimone, Italy	2200	^c 2007-2009	17.20(14.30)	2.45(2.00)		--	Andrews et al. (2011)
Moussala Peak, Bulgaria	2400	^e 2007-2009	16.00(12.20)		2.20(2.12)	--	Andrews et al. (2011)
NCO-P	5079	^f 2006-2008	17.40(10.70)	1.63(0.97)	1.59(1.22)	--	Andrews et al. (2011)
Mount Waliguan China	3800	^a 2005-2008	42.50(39.70)	2.31(1.94)	0.89(0.85)	--	Andrews et al. (2011)
Lulin Mountain, Tiwan	2900	^a 2008-2009	25.80(10.80)	2.83(0.97)	1.57(1.51)	--	Andrews et al. (2011)
Montsec, W. Mediter.	1570	Jun-11 – Jun-13	25.4 ± 27.5	1.5 ± 1.4	1.56 ± 0.88	--	Pandolfi et al. (2014)
Cape Cod, MA	20	Jul-12-Jul-13	22 ± 15	1.1 ± 0.9	1.8 ± 0.6	--	Titos et al. (2014a)
Granada, Spain	680	Winter 2013	41 ± 34	17 ± 17	1.8 ± 0.4	--	Titos et al. (2014b)
Granada, Spain		Spring 2013	38 ± 26	11 ± 11	1.8 ± 0.3		Titos et al. (2014b)

934

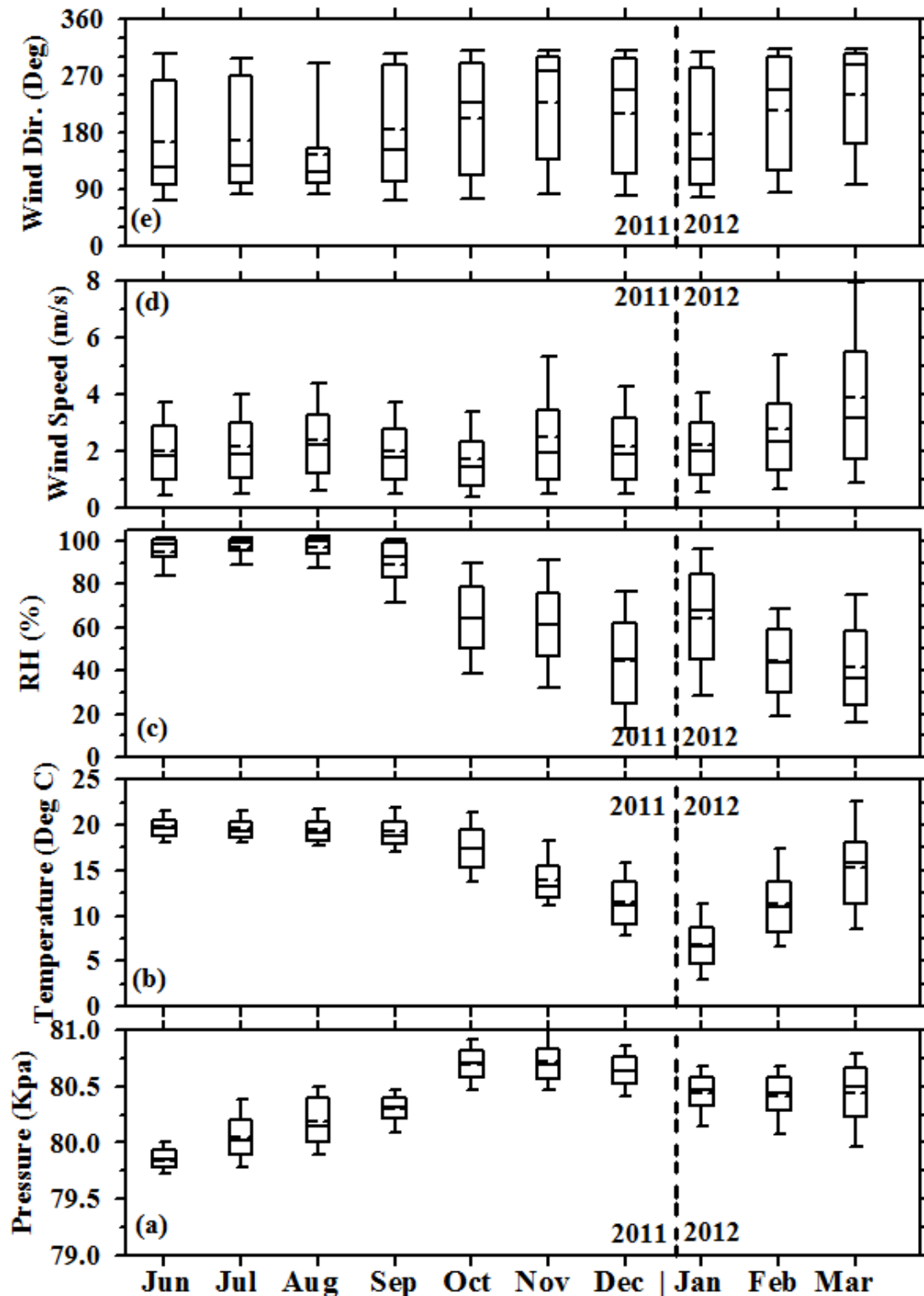
935 * Value inside parenthesis represents for $D_{1\mu\text{m}}$ size aerosols

936 **Value Excluding Saharan dust event (SDE)

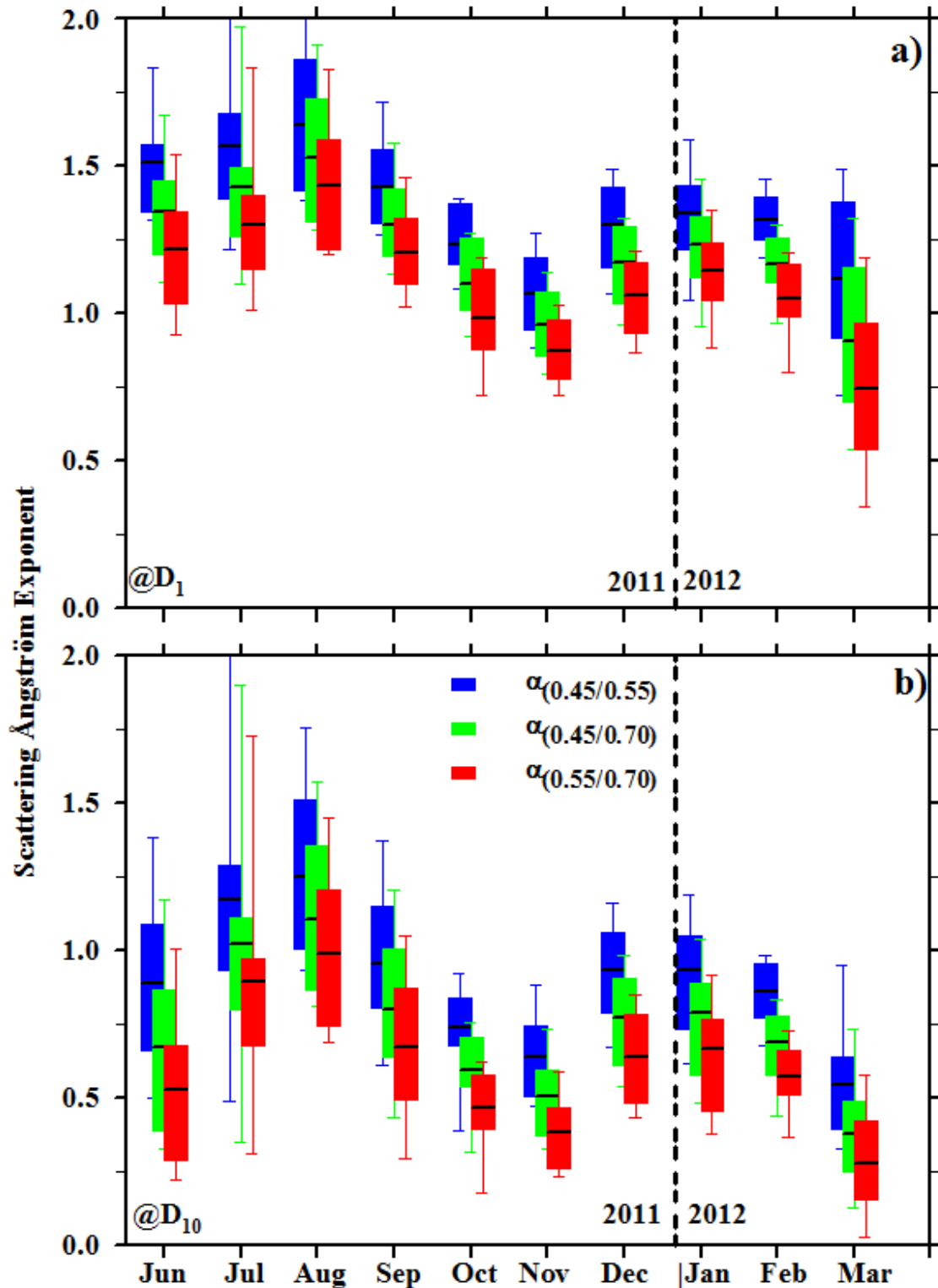
937 *** Value Exclusively for Saharan dust event (SDE)

938 ^aSize cut (10 μm); ^bSize cut (2.5 μm); ^cSize cut (1.0 μm); ^dSize cut (7.0 μm); ^e Whole air; ^fSize cut (2.5 μm for scattering) and Size cut (10.0 μm for absorption)

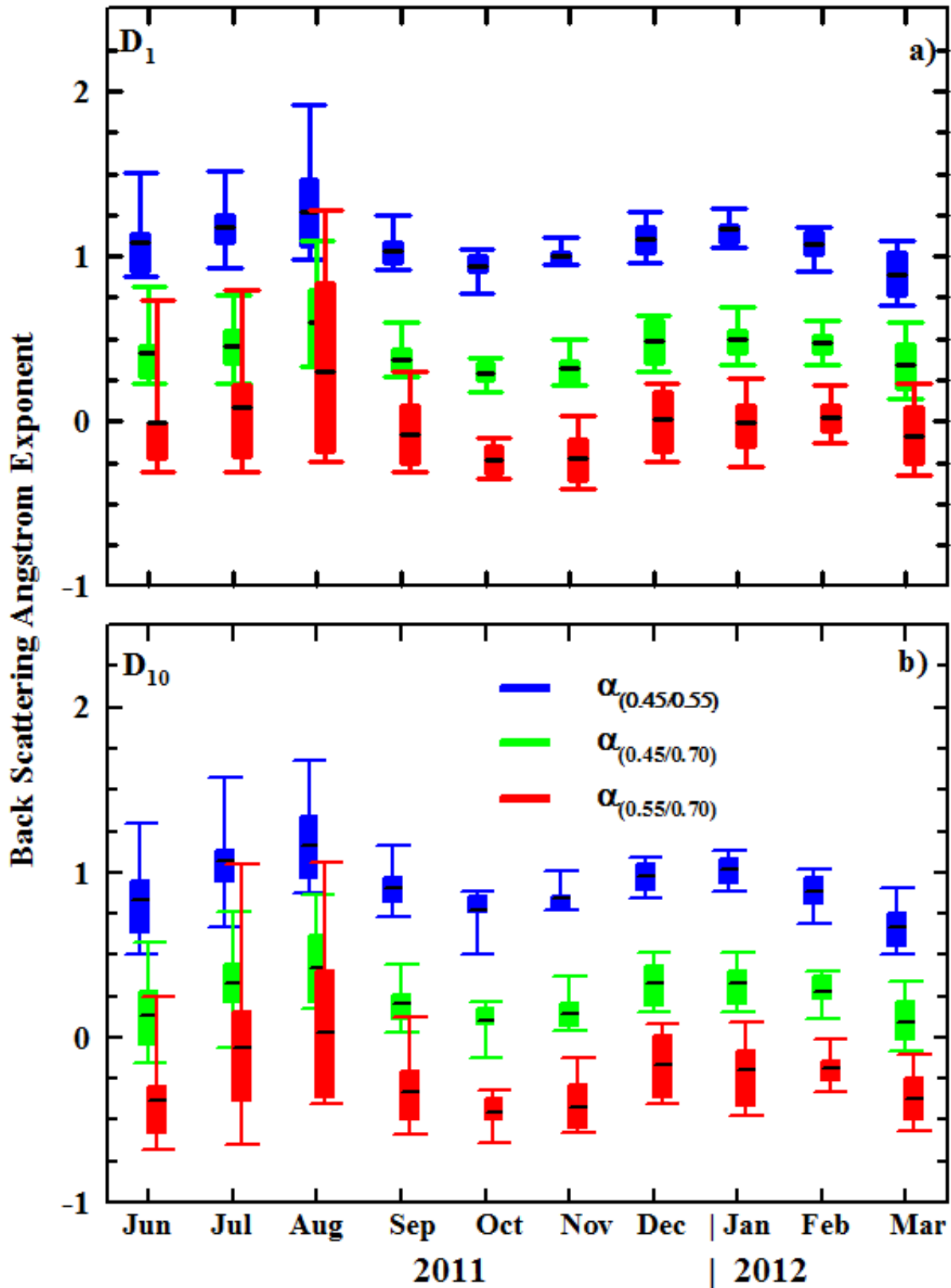
940 Values taken from Andrews et al. (2011) are in STP and value inside the bracket represents for free troposphere



941
 942 **Figure 1:** Monthly surface meteorological variables (ambient pressure, air Temperature, Relative
 943 Humidity, wind speed and direction) at Nainital during the period June 2011 to March 2012 in
 944 box and whisker charts. The dashed line represents the mean and the solid line the median. The
 945 box contains the range of values from 25% (bottom) to 75% (top).



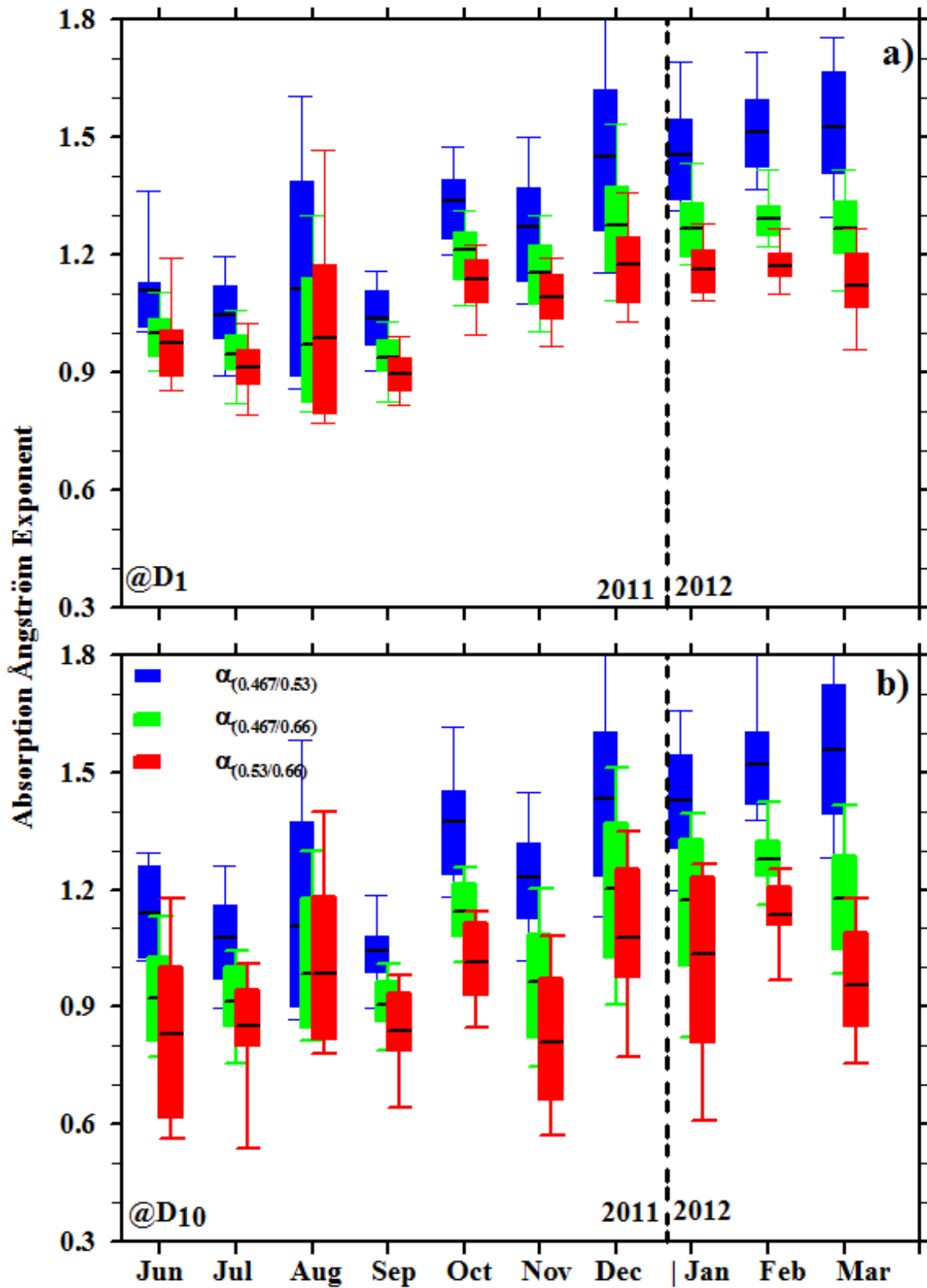
946
 947 **Figure 2:** Monthly-mean variation of scattering Ångström exponent for $D_{1\mu\text{m}}$ (a) and $D_{10\mu\text{m}}$ (b)
 948 during June 2011 to March 2012. The box and whiskers denote the 95th and 5th percentiles,
 949 respectively. The box's upper and lower limits are 75th and 25th percentiles and black straight
 950 line shows the mean value. The vertical dotted line separates the years 2011 and 2012.



951

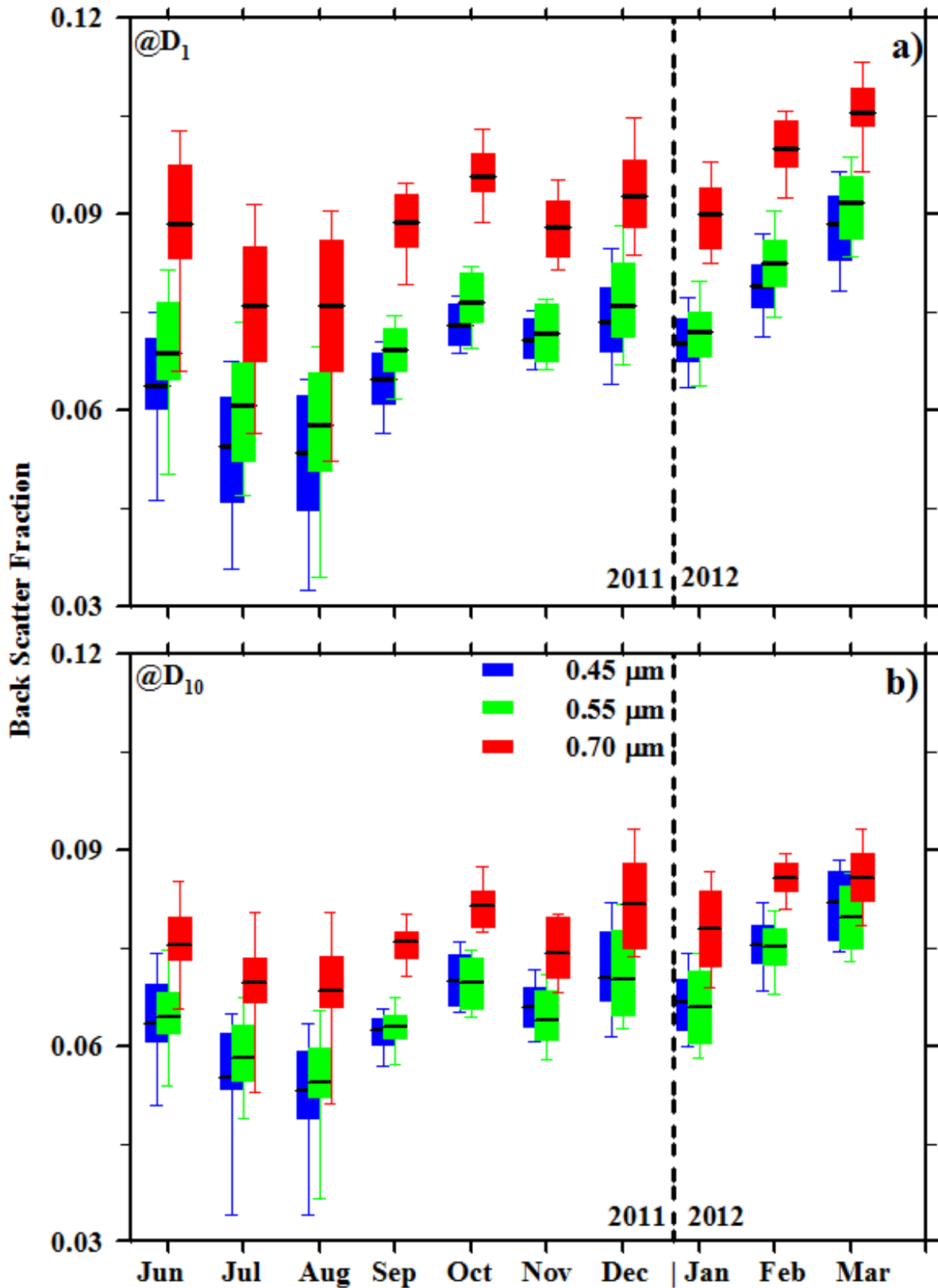
952

Figure 3: Same as in Figure 2, but for the back-scattering Ångström exponent.



953

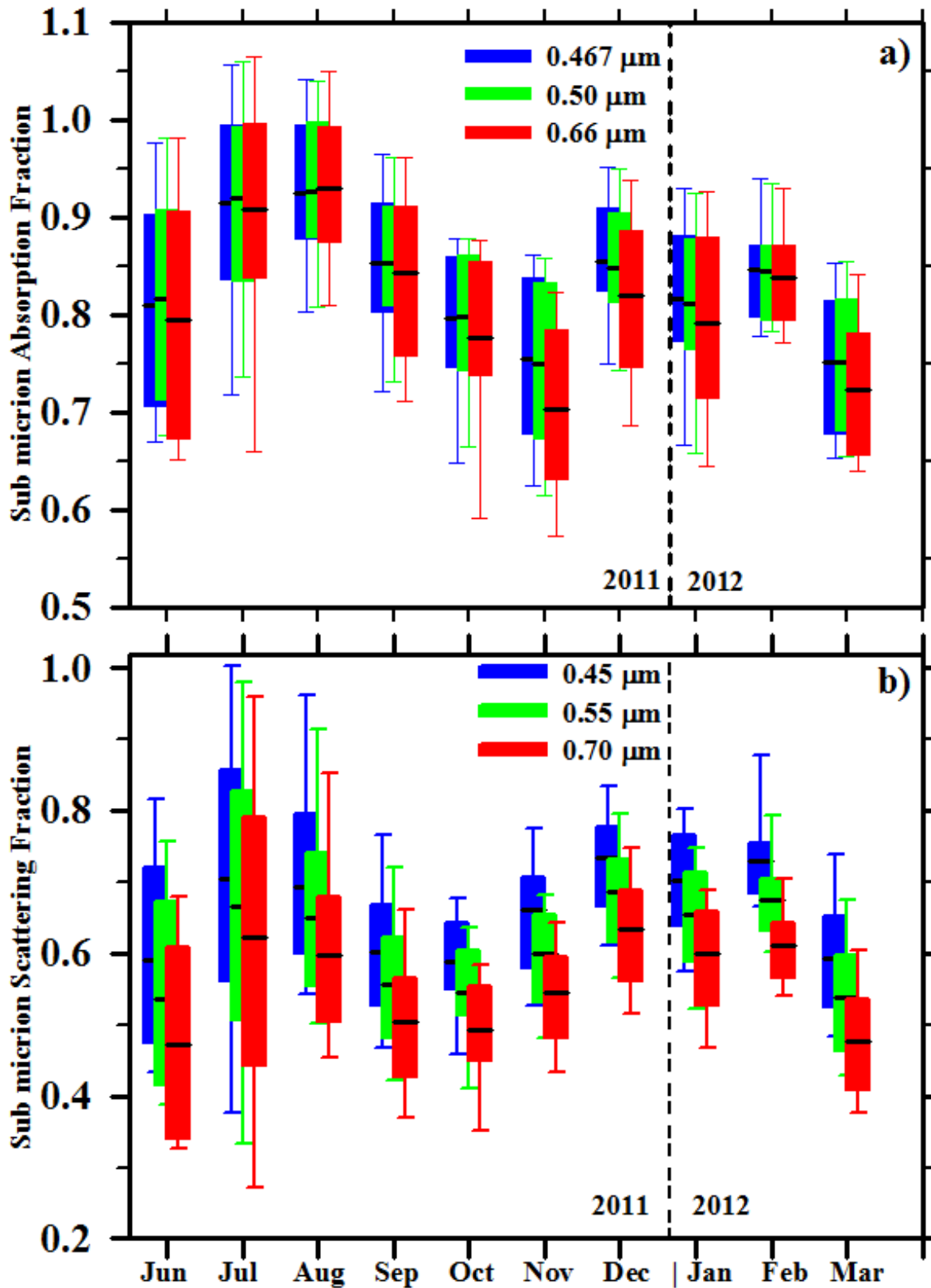
954 **Figure 4:** Same as in Figure 2, but for the absorption Ångström exponent.



955

956

Figure 5: Same as in Figure 2, but for the back-scatter fraction.

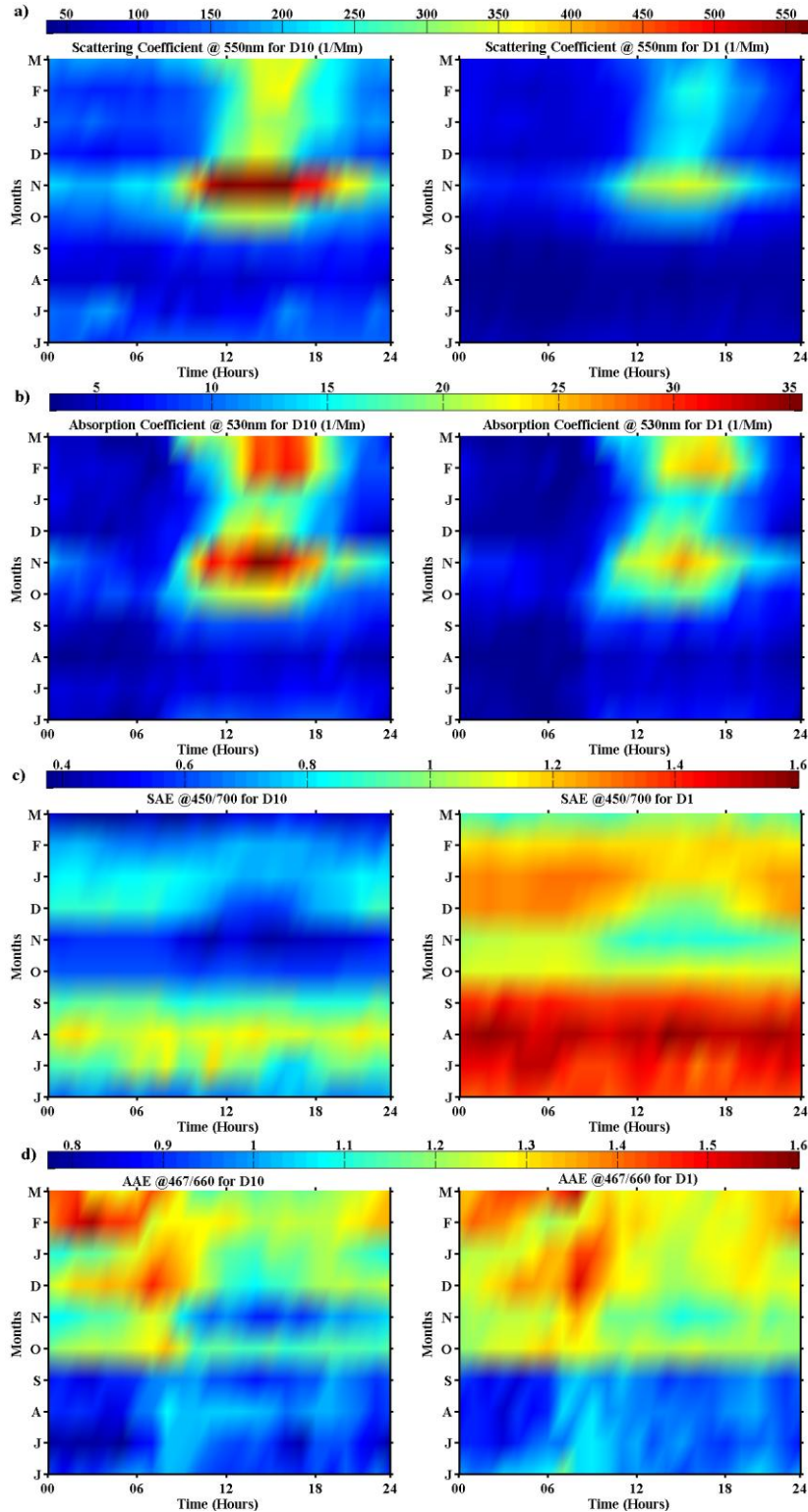


957

958

Figure 6: Same as in Figure 2, but for the sub-micron absorption (a) and scattering (b) fraction.

959



960

961

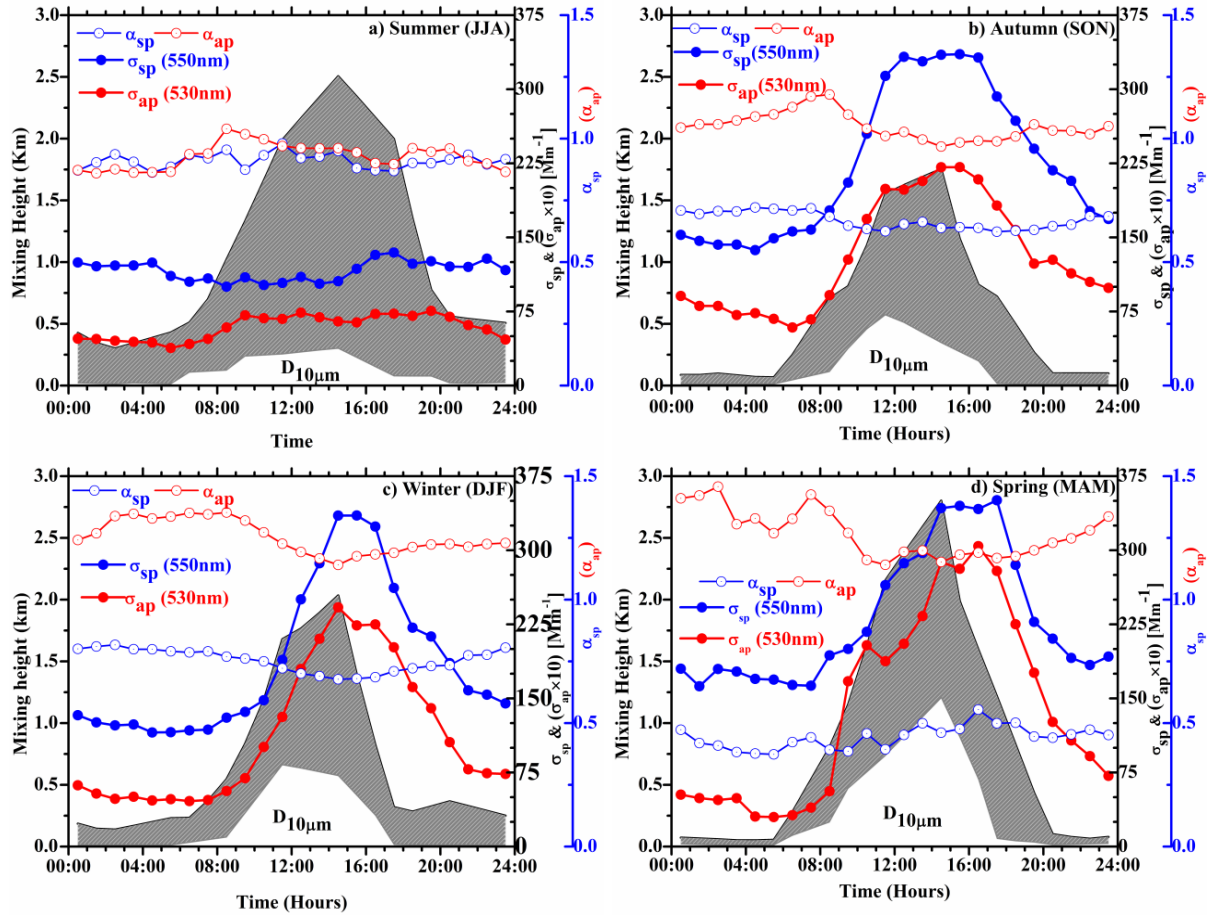
962

963

964

965

Figure 7: Monthly mean diurnal variation of (a) scattering coefficient, (b) absorption coefficient, (c) Scattering Ångström Exponent (SAE) and, (d) Absorption Ångström Exponent (AAE) for D_{10µm} and D_{1µm} size particles.



966

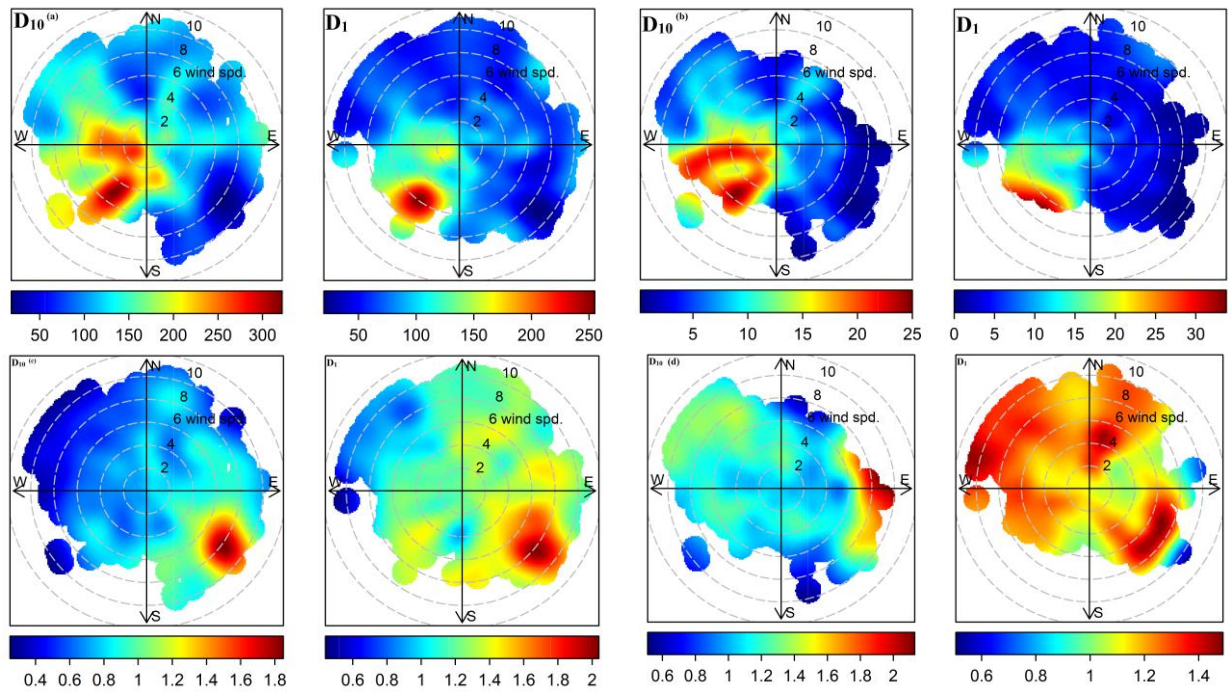
967

968 **Figure 8:** Diurnal variation of the seasonal mean scattering, absorption coefficients, SAE and
 969 AAE for $D_{10\mu\text{m}}$ particles along with respective variations in the maximum and minimum mixing-
 970 layer height over Nainital. The absorption coefficient was multiplied by 10.

971

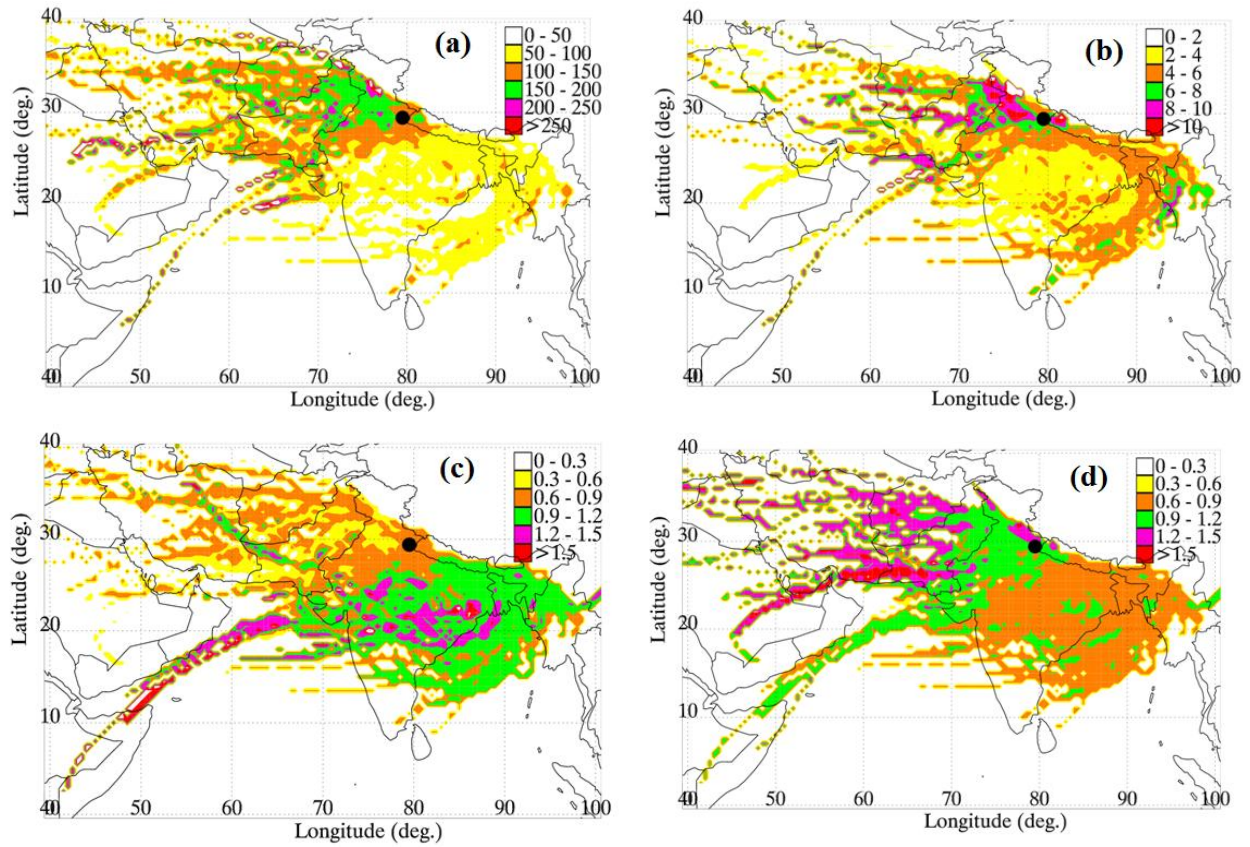
972

973

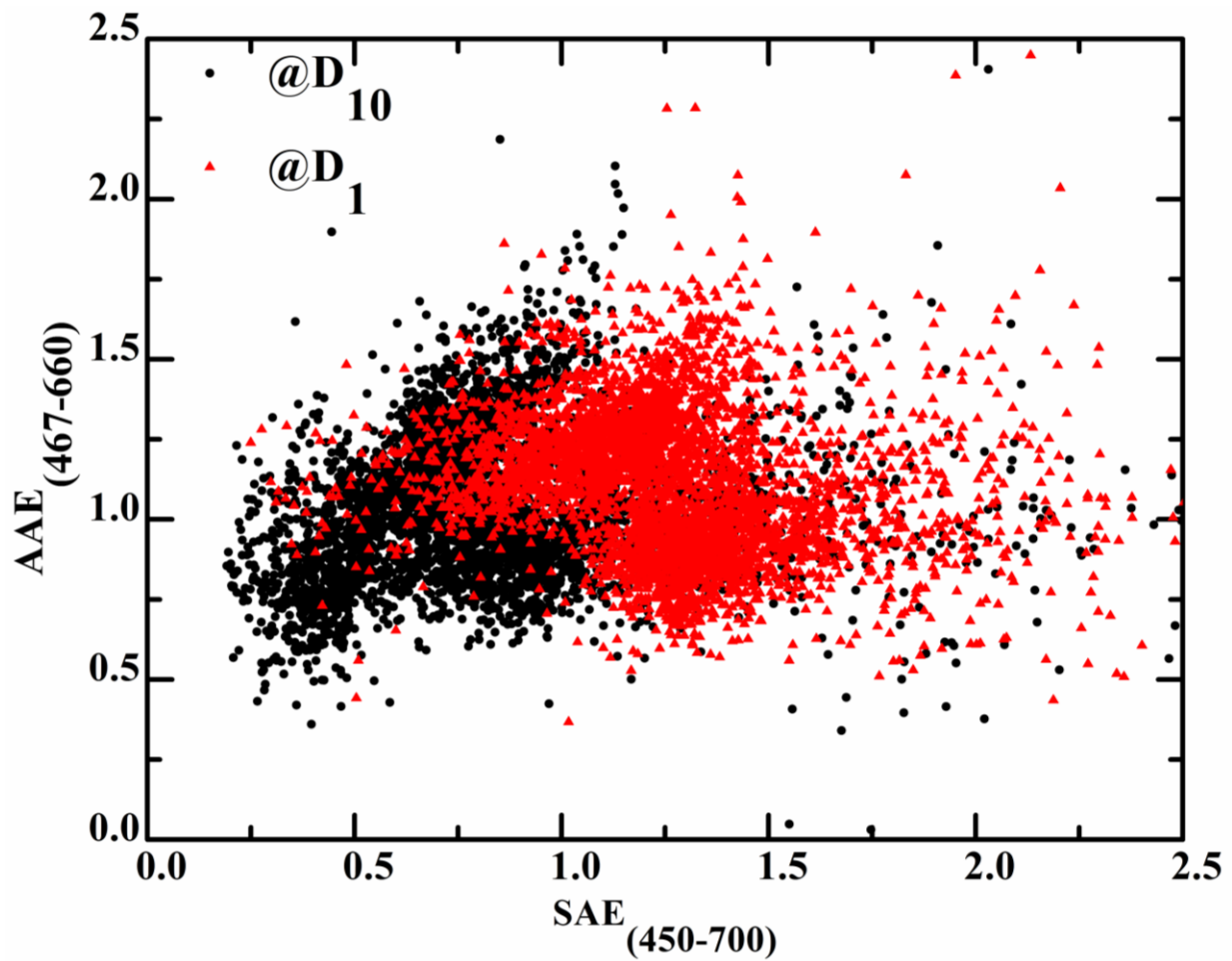


975 **Figure 9:** Bivariate plots of the scattering coefficient (a), absorption coefficient (b), scattering
 976 Ångström exponent (c) and absorption Ångström exponent (d) for $D_{10\mu m}$ and $D_{1\mu m}$ size groups.

977
 978
 979
 980
 981
 982
 983
 984
 985
 986
 987
 988
 989
 990
 991
 992
 993



994 **Figure 10:** Concentrated Weighted Trajectory (CWT) maps using 5-days backward trajectories
 995 ending at Nainital at 500 m for scattering (a), absorption (b) coefficients, SAE (c) and AAE (d)
 996 for $D_{10\mu\text{m}}$ particles.



997
 998 **Figure 11:** Correlation between scattering and absorption Ångström exponents (hourly-averaged
 999 values) at Nainital for $D_{1\mu\text{m}}$ and $D_{10\mu\text{m}}$ particle-size groups.